HAL open science

Tokamak free-boundary plasma equilibrium computation using finite elements of class C0 and C1 within a mortar element approach

Ali Elarif, Blaise Faugeras, Francesca Rapetti

▶ **To cite this version:**

Ali Elarif, Blaise Faugeras, Francesca Rapetti. Tokamak free-boundary plasma equilibrium computation using finite elements of class C0 and C1 within a mortar element approach. Journal of Computational Physics, 2021, 439, pp.110388. 10.1016/j.jcp.2021.110388 . hal-02955007

HAL Id: hal-02955007

https://inria.hal.science/hal-02955007v1

Submitted on 1 Oct 2020

HAL is a multi-disciplinary open access archive for the deposit and dissemination of scientific research documents, whether they are published or not. The documents may come from teaching and research institutions in France or abroad, or from public or private research centers.

L'archive ouverte pluridisciplinaire **HAL**, est destinée au dépôt et à la diffusion de documents scientifiques de niveau recherche, publiés ou non, émanant des établissements d'enseignement et de recherche français ou étrangers, des laboratoires publics ou privés.

Tokamak free-boundary plasma equilibrium computation using finite elements of class $\mathcal{C}^0$ and $\mathcal{C}^1$ within a mortar element approach

Ali Elarif, Blaise Faugeras, Francesca Rapetti

RESEARCH REPORT
N° 9364
Oct. 2020
Project-Team CASTOR

ISSN 0249-6399 ISRN INRIA/RR--9364--FR+ENG

Tokamak free-boundary plasma equilibrium computation using finite elements of class $\mathcal{C}^0$ and $\mathcal{C}^1$ within a mortar element approach

Ali Elarif, Blaise Faugeras, Francesca Rapetti

Project-Team CASTOR

Research Report n° 9364 — Oct. 2020 — 28 pages

Abstract: The numerical simulation of the equilibrium of the plasma in a tokamak as well as its self-consistent coupling with resistive diffusion should benefit from higher regularity of the approximation of the magnetic flux map. In this work, we propose a finite element approach on a triangular mesh of the poloidal section, that couples piece-wise linear finite elements in a region that does not contain the plasma and reduced Hsieh-Clough-Tocher finite elements elsewhere. This approach gives the flexibility to achieve easily and at low cost higher order regularity for the approximation of the flux function in the domain covered by the plasma, while preserving accurate meshing of the geometric details in the rest of the computational domain. The continuity of the numerical solution at the coupling interface is weakly enforced by mortar projection. A new technique for the computation of the geometrical coefficients is also presented.

Key-words: Tokamak, equilibrium, reduced Hsieh-Clough-Tocher finite element, Newton method, geometrical coefficients

RESEARCH CENTRE
SOPHIA ANTIPOLIS – MÉDITERRANÉE

2004 route des Lucioles - BP 93
06902 Sophia Antipolis Cedex

Résumé : La simulation numérique de l'équilibre du plasma dans un tokamak et du couplage avec la diffusion resistive devrait bénéficier d'une plus grande régularité de l'approximation du flux magnétique. Dans ce travail nous proposons une approche par éléments finis sur un maillage triangulaire de la section poloidale, couplant éléments finis linéaires par morceaux dans une region ne contenant pas le plasma et éléments finis de Hsieh-Clough-Tocher réduits ailleurs. Cette approche permet facilement d'obtenir une régularité d'ordre élevé de l'approximation de la fonction flux dans le domaine couvert par le plasma, tout en préservant un maillage précis des structures géométriques dans le reste du domaine. La continuité de la solution numérique à l'interface de couplage est imposée de manière faible par projection de mortar. Une nouvelle méthode pour le calcul des coefficients geométriques du plasma est également présentée.

Mots-clés : tokamak, équilibre, elements finis de Hsieh-Clough-Tocher réduits, méthode de Newton, coefficients geométriques

Contents

1 Introduction **4**

2 Free-boundary Grad-Shafranov equation **5**

3 Variational formulation **8**

4 Coupling different finite elements on non-overlapping meshes **10**
4.1 The finite element spaces 10
4.2 The discrete coupling condition 12
4.2.1 The interpolation case 12
4.2.2 The L^2-projection case 12
4.2.3 The discrete problem 14

5 The discrete problem in matrix form **15**

6 Computation of geometric coefficients **17**
6.1 The iso-contour method 17
6.2 The weak formulation method 18

7 Numerical results **19**
7.1 Validation of rHCT FE implementation 19
7.2 JT60-SA tokamak test case 20

8 Conclusion **24**

1 Introduction

The way a magnetic field influences the transport properties of charged particles is of high interest for a wide spectrum of physical systems and areas. It is a complex challenging problem that goes beyond the purpose of the present paper. However, its suggests some key ingredients that need to be correctly treated from the mathematical and numerical points of view.

Among the ingredients we first have the computation of the equilibrium of a plasma in a Tokamak (see for example [22] and the references therein). It is a free boundary problem described by the Grad-Shafranov equation in axisymmetric configuration (see more details in [6]). The right-hand side of this equation is a nonlinear source, which represents the toroidal component of the plasma current density. On the numerical side, the use of finite elements (FEs) enables an accurate resolution of complicated geometric features of realistic tokamak devices, while Newton methods are involved to solve the resulting nonlinear finite-dimensional systems thus ensuring fast convergence. The Newton schemes are highly non-trivial, since the domain covered by the plasma is unknown and depends non-linearly on the poloidal magnetic flux, ψ, the primal unknown. Boundary conditions at infinity are consistently incorporated through boundary integral equations [13]. Another ingredient is the correct simulation of the transport in the plasma which is rather complex due to the presence of turbulence at the plasma edge and of thermal exchanges with the chamber wall (see [6], [11]).

An aspect linking the two previous ones is the precise computation of the magnetic configuration and of 1D averaged quantities, which is the object of the present work. In tokamaks the energy and particle transport is anisotropically distributed, that is, along magnetic surfaces it is much greater than across the magnetic surfaces. We can thus assume that densities and temperatures are constant on each magnetic surface. If we label by ρ the magnetic surface S, we define the average over S of a given quantity u by $\langle u \rangle = \partial_V (\int_S u \, dV) = \frac{1}{V'} \int_S u \frac{dS}{|\nabla \rho|}$ where $V' = \partial_\rho V$ and V is the volume enclosed inside the surface S. The derivative $\partial_\rho V$ can be computed once suitable 1D profiles (such as, for example, $\partial_\rho \psi$ or $\partial_\psi \rho$) are known. These 1D profiles, among which the so-called *geometric coefficients* have to be computed with care. They are important functionals of the solution of such equilibrium problems that are essential to incorporate resistive diffusion effects into plasma evolution modeling [18, 24, 6, 26]. Also many plasma characteristics (e.g. the so-called safety factor or the average current density profile), important to quantify stability or for monitoring during the experiment, are defined as integrals involving the gradient $\nabla \psi$ of the poloidal flux.

In order to improve the description of $\nabla \psi$ we wish to introduce in certain parts of the computational domain, FE functions that are not only continuous, but have also first order continuous derivatives. For this purpose, instead of relying on composite meshes [23], we consider a non-overlapping domain decomposition formulation of the physical problem and couple, by means of mortar projection [3, 4], reduced Hsieh-Clough-Tocher (rHCT) FEs [9, 8] in the plasma domain to piece-wise linear Lagrange FEs in the exterior domain. These rHCT FEs have the advantage to be defined on triangles and to be less expensive from a computational point of view than quintic FEs used in [25]. Concerning the computation of geometric coefficients, we propose and compare two strategies. The first one, rather usual in equilibrium codes, relies on the explicit computation of iso-contours. The second one which proves to be very efficient is based on the coarea formula and motivated by results from [10].

The paper is organised as follows. Section 2 briefly introduces the equations modelizing the equilibirum of the plasma in a tokamak. In Section 3 we introduce the associated variational formulation in a non-overlapping domain decomposition framework. Section 4 exposes the finite elements used and the proposed coupling method. In Section 5 we move to the fully discretized problem and the implemented Newton method. Section 6 presents the numerical methods pro-

posed for the computation of geometric coefficents, and in Section 7 we show numerical results and as an example apply the method to the computation of an equilibrium in the JT60-SA tokamak.

2 Free-boundary Grad-Shafranov equation

The equations which govern the equilibrium of a plasma in presence of a magnetic field in a tokamak are the solenoidal condition and Ampère's law in the whole space (including the plasma) and the force balance in the plasma itself, which read, respectively,

$$\operatorname{div} \mathbf{B} = 0, \qquad \mathbf{curl}\, \frac{1}{\mu}\mathbf{B} = \mathbf{J}, \qquad \mathbf{grad}\, p = \mathbf{J} \times \mathbf{B}, \tag{1}$$

where p is the plasma kinetic pressure, $\mathbf{B}$ is the magnetic induction, $\mathbf{J}$ is the current density and μ the magnetic permeability. These equations are sufficient for the modeling of the plasma static equilibrium. To simulate the plasma quasi-static evolution, the set of equations (1) has to be completed with also Faraday's law in all the conducting structures, and Ohm's laws in the plasma, coils and passive structures. Assuming axial symmetry in the geometry of the tokamak, we may introduce a cylindrical coordinate system (r, φ, z), such that $r = 0$ is the major axis of the tokamak torus. We recall that the transformation $x = r\cos\varphi$ and $y = r\sin\varphi$ allows to pass from cylindrical coordinates (r, φ, z) to Cartesian ones (x, y, z). Equations (1) are reformulated in a (poloidal) section $\varphi =$ constant of the tokamak, making the hypothesis that the scalar field p does not depend on the angle φ, thus $\mathbf{grad}\, p$ belongs to the poloidal (r, z)-plane. The classical primal unknowns for toroidal plasma equilibria described by (1) are the *poloidal magnetic flux* $\psi = \psi(r, z)$, the pressure p and the *diamagnetic function* f. The poloidal magnetic flux $\psi := r\mathbf{A}\cdot\mathbf{e}_\varphi$ is the scaled toroidal component (φ-component) of the magnetic vector potential $\mathbf{A}$, such that $\mathbf{B} = \mathbf{curl}\, \mathbf{A}$, where $\mathbf{e}_\varphi$ denotes the unit vector for the φ coordinate. Note that $\mathbf{A}$ is divergence-free (Coulomb gauge) by construction. The diamagnetic function $f = r\mathbf{B}\cdot\mathbf{e}_\varphi$ is the scaled toroidal component of the magnetic induction $\mathbf{B}$. The magnetic induction $\mathbf{B}$ can thus be represented as

$$\mathbf{B} = \mathbf{B}_{pol} + \mathbf{B}_{tor}, \qquad \mathbf{B}_{pol} = \frac{1}{r}\nabla\psi \times \mathbf{e}_\varphi, \qquad \mathbf{B}_{tor} = B_\varphi \mathbf{e}_\varphi = \frac{f}{r}\mathbf{e}_\varphi$$

as it is assumed to be independent of the angle φ, where ∇ is the gradient operator in the r, z coordinates. The previous relations show that the magnetic surfaces are generated by the rotation of the iso-flux lines around the axis of the torus. We refer to standard text books, e.g. [15], [6], [34], [17], [16] and [26] for the details and state in the following only the final equations.

We introduce $\Omega_\infty = [0, \infty] \times [-\infty, \infty]$, the positive half plane, to denote the meridian plane that contains the poloidal section of the tokamak, centered at the origin. In axisymmetric coordinates, force balance, the solenoidal condition and Ampère's law in (1) yield the following equation for the flux $\psi(r, z)$ in Ω_∞

$$-\Delta^*\psi = \mathrm{J}_\varphi, \tag{2}$$

where $\mathrm{J}_\varphi\mathbf{e}_\varphi$ is the toroidal component of $\mathbf{J}$, and the second order elliptic differential operator $-\Delta^*$ is defined by

$$-\partial_r\left(\frac{1}{\mu(\psi)r}\partial_r\psi\right) - \partial_z\left(\frac{1}{\mu(\psi)r}\partial_z\psi\right) := -\Delta^*\psi \tag{3}$$

where $\mu(\psi)$ is the magnetic permeability, which is equal to μ_0, the constant permeability of the vacuum, everywhere except in the possibly existing iron parts of the tokamak (see Figure 1). The geometry of the tokamak determines various subdomains (see Figure 1) which are then used to specify J_φ accordingly:

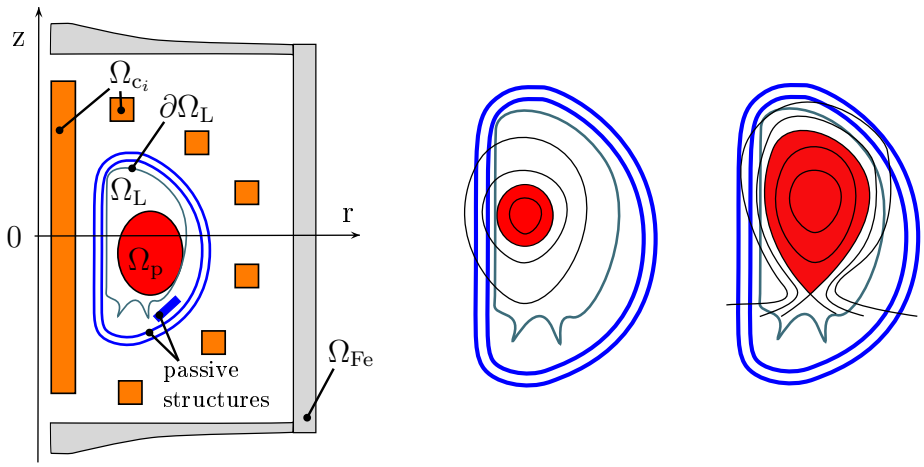

Figure 1: Left: Geometric description of the tokamak in the poloidal plane. Middle and right: Sketch for characteristic plasma shapes. The plasma boundary touches the limiter (middle) or the plasma is enclosed by the separatrix, a flux line that goes through an X-point (right).

- $\Omega_{\rm Fe} \subset \Omega_\infty$ denotes those parts of Ω_∞ made of iron where the permeability μ is not constant and given as a (non-linear) function of ψ, namely $\mu(\psi) = \mu_{Fe}(|\nabla\psi|^2 r^{-2})$; if $\Omega_{\rm Fe} = \emptyset$, then $\mu = \mu_0$ everywhere;
- $\Omega_{c_i} \subset \Omega_\infty$, $1 \le i \le N_c$, denotes the intersection of the ith coil with the poloidal plane. We suppose that ith coil has n_i wire turns and cross section area $|\Omega_{c_i}|$;
- $\Omega_{\rm L} \subset \Omega_\infty$, denotes the domain bounded by the limiter, thus the domain accessible by the plasma;
- $\Omega_{\rm p} \subset \Omega_{\rm L}$, denotes the domain covered by the plasma and the boundary $\partial\Omega_{\rm p}$ is the outermost closed ψ-isocontour contained within the limiter region $\Omega_{\rm L}$.

The toroidal component of the current density J_φ is zero everywhere outside the plasma domain and the poloidal field coils (and possibly the passive structures).
In the coils Ω_{c_i}, we set $J_\varphi = \frac{I_i}{|\Omega_{c_i}|}$, where I_i is the total current (in At, ampère turns) in the ith coil. In the static modeling, I_i is constant whereas in the quasi-static case I_i is related to assigned tensions $v_i(t)$ in the supplies and to mutual and self inductance via electric circuit equations, as explained in [22].
In the passive structures, we set $J_\varphi = 0$ for static equilibrium computations whereas for the quasi-static evolution of the equilibrium we need to set $J_\varphi = -(\sigma/r)\partial_t\psi$ where σ is the electric conductivity of the passive structures.
In the plasma domain $\Omega_{\rm p}$, the equations (1) imply that both the pressure p and the diamagnetic function f are constant on each ψ-isoline, *i.e.*, $p = p(\psi)$ and $f = f(\psi)$. One then deduces the so-called Grad-Shafranov-Schlüter equilibrium equation in the plasma [19], [31], [27]

$$-\Delta^*\psi = rp'(\psi) + \frac{1}{\mu_0 r} f f'(\psi) \tag{4}$$

where the right-hand side of equation (4) is the toroidal component J_φ of the plasma current density. Functions p' and ff', that are zero outside $\Omega_{\rm p}$, are non-linear with respect to ψ. They

can be either reconstructed starting from field measures (this is the goal of the inverse equilibrium reconstruction problem) or supplied as data (in the direct equilibrium problem). In the latter case, we need to introduce few additional notations.

The plasma domain $\Omega_{\rm p}(\psi)$ is unknown and depends non-linearly on the poloidal flux ψ, in other words, $\Omega_{\rm p} = \Omega_{\rm p}(\psi)$ is a functional of the poloidal flux ψ (and we have a free-boundary problem). The different characteristic shapes of $\Omega_{\rm p}(\psi)$ are illustrated in Figure 1: the boundary of $\Omega_{\rm p}(\psi)$ either touches $\partial\Omega_{\rm L}$ the boundary of $\Omega_{\rm L}$ (limiter configuration) or contains one or more saddle points of ψ (divertor configuration). In the latter case, the boundary of the plasma domain is named the magnetic separatrix. The saddle points of ψ, denoted by $(r_{\rm X}, z_{\rm X})$=$(r_{\rm X}(\psi), z_{\rm X}(\psi))$, are called X-points of ψ. The plasma domain $\Omega_{\rm p}(\psi)$ is the largest subdomain of $\Omega_{\rm L}$ bounded by a closed ψ-isoline in $\Omega_{\rm L}$ and containing the magnetic axis (r_a, z_a). The magnetic axis is the point $(r_a, z_a) = (r_a(\psi), z_a(\psi))$, where ψ has its global maximum (or minimum, depending on axis positive direction) in $\Omega_{\rm L}$. For convenience, we introduce also the coordinates $(r_b, z_b) = (r_b(\psi), z_b(\psi))$ of the point that determines the plasma boundary. Note that (r_b, z_b) is either an X-point of ψ or the contact point with $\partial\Omega_{\rm L}$.

The domain of p' and $f\,f'$ is the interval $[\psi_a, \psi_b]$, with the scalar values ψ_a and ψ_b being the flux values at the *magnetic axis* and at the boundary of the plasma (supposing $\psi_a < \psi_b$):

$$\begin{aligned} \psi_a(\psi) &:= \psi(r_a(\psi), z_a(\psi))\,, \\ \psi_b(\psi) &:= \psi(r_b(\psi), z_b(\psi))\,. \end{aligned} \tag{5}$$

Since the domain of p' and $f\,f'$ depends on the poloidal flux itself, it is more practical to supply these profiles as functions of the normalized poloidal flux $\psi_{\rm N}(r, z)$:

$$\psi_{\rm N}(r, z) = \frac{\psi(r, z) - \psi_a(\psi)}{\psi_b(\psi) - \psi_a(\psi)}\,. \tag{6}$$

These two functions, subsequently termed $S_{p'}$ and $S_{ff'}$, have, independently of ψ, a fixed domain $[0, 1]$. They are usually given as piecewise polynomial functions. Another frequent a priori model is

$$S_{p'}(\psi_{\rm N}) = \lambda\frac{\beta}{r_0}(1 - \psi_{\rm N}^{\alpha})^{\gamma}\,, \quad S_{ff'}(\psi_{\rm N}) = \lambda(1 - \beta)\mu_0 r_0(1 - \psi_{\rm N}^{\alpha})^{\gamma}\,, \tag{7}$$

with r_0 the characteristic radius (in meters) of the tokamak vacuum chamber and $\alpha, \beta, \gamma \in \mathbb{R}$ given parameters. The parameter β is related to the poloidal beta [6, p. 15], whereas α and γ describe the peakage of the current profile, λ is a scaling parameter related to the total plasma current. In the following we use the formulation

$$\mathrm{J}_{\varphi} = \lambda(\frac{r}{r_0}\mathcal{A}(\psi_{\rm N}) + \frac{r_0}{r}\mathcal{B}(\psi_{\rm N}))$$

with $\mathcal{A} = r_0 S_{p'}$ and $\mathcal{B} = \dfrac{1}{r_0\mu_0}S_{ff'}$ given functions on $[0, 1]$.

Equilibrium equation (2) can be either considered in the whole poloidal plane Ω_∞, with $\lim_{||(r,z)||\to+\infty}\psi(r, z) = 0$ as boundary condition at infinity and $\psi(0, z) = 0$ at the axis $r = 0$, or in a restricted bounded domain Ω_{re}, as in Figure 2 (right). In this second case, the boundary of Ω_{re} can be viewed as a measurement contour Γ including $\Omega_{\rm L}$, and possibly some of the coils and passive structures, with $\psi(r, z)$ assigned for all points (r, z) on the boundary of Ω_{re}. Suitable initial conditions on ψ should be added in case we were interested by the quasi-static evolution problem (see [12]). In this paper, we restrict ourselves to static equilibrium computations for an iron-free tokamak.

As we are going to present later a discretization scheme for the problem (2) that employs different approximation spaces on the tokamak poloidal section Ω_∞, we formulate the variational problem in a bounded spatial domain $\Omega \subset \Omega_\infty$ directly in a non-overlapping domain decomposition framework.

3 Variational formulation

There are two possible ways to define a computational domain $\Omega \subset \Omega_\infty$ to be triangulated. It can either be a restricted domain Ω_{re} enclosed in the measurement contour Γ with $\Omega_{\mathrm{L}} \subset \Omega_{re}$, as in Figure 2 (right), or a sufficiently large semi-circle centered at the origin and containing the whole poloidal section of the tokamak, as in Figure 2 (left). The first case is called the bounded domain case and the second the ABB domain case, that bears its name from Albanase, Blum, de Barbieri, who first introduced in [1] the boundary integral method on the semi-circle used to take into account conditions at infinity. In the following, we work with the ABB domain.

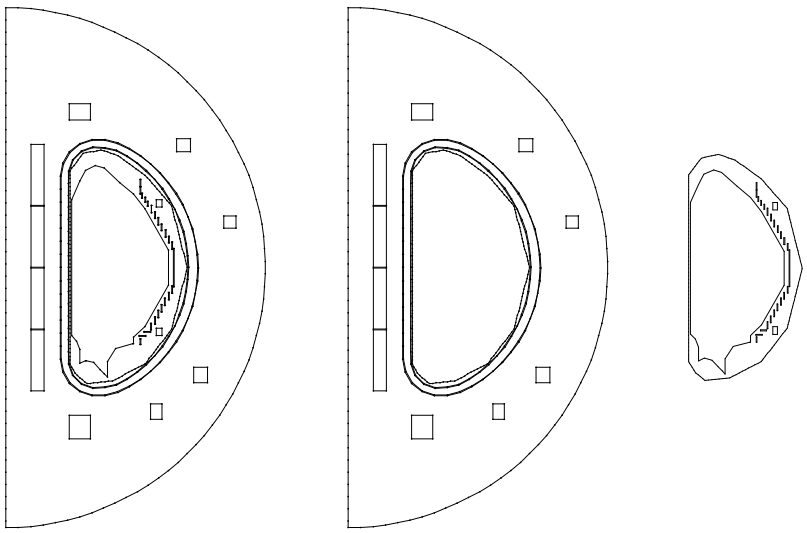

Figure 2: The global ABB configuration containing the poloidal section of the JT60SA tokamak (left), as union of two subdomains, namely the external part not containing Ω_{L} (center) and the internal part containing Ω_{L} (right).

To define the ABB domain, we choose a semi-circle γ of radius ρ_γ surrounding all the coil domains Ω_{c_i}. The ABB domain $\Omega \subset \Omega_\infty$, that is used for computations, has boundary $\partial\Omega = \gamma \cup \gamma_0$, where $\gamma_0 := \{(0,z),\, -\rho_\gamma \le z \le \rho_\gamma\}$. We have now to select the functional space where the unknown ψ lives. We recall that the coordinates (r, z, φ) vary in $\tilde{\Omega} = \Omega \times [0, 2\,\pi] \subset \mathbb{R}^3$ and $\psi(r,z) = rA_\varphi(r,z)$ where $\mathbf{A} = (0, 0, A_\varphi)^\top$ is the magnetic vector potential. The vector potential $\mathbf{A}$ has to be selected in $H(\mathbf{curl}, \tilde{\Omega})$, the space of vector fields in $L^2(\tilde{\Omega})^3$ with $\mathbf{curl}$ in $L^2(\tilde{\Omega})^3$. We thus need to have:
(i) $[\mathbf{A} \times \mathbf{n}]_{\mathcal{I}} = \mathbf{0}$, that is the continuity of the tangential trace of $\mathbf{A}$ across any interface $\mathcal{I} \subset \Omega$. This condition is associated with $[\mathbf{B} \cdot \mathbf{n}]_{\mathcal{I}} = 0$, the continuity of the normal component of $\mathbf{B}$ across $\mathcal{I}$. Since $\mathbf{A} = A_\varphi\, \mathbf{e}_\varphi$ whereas $\mathbf{n}$, the normal vector to $\mathcal{I}$, is in the poloidal section Ω, it is sufficient to have A_φ continuous across $\mathcal{I}$. The transmission condition $[\frac{1}{\mu}\mathbf{curl}\,\mathbf{A} \times \mathbf{n}]_{\mathcal{I}} = \mathbf{0}$, associated with

$[\mathbf{H}\times\mathbf{n}]_{\mathcal{I}}=\mathbf{0}$, the continuity of the tangential trace of the magnetic field $\mathbf{H}=(1/\mu)\mathbf{B}$ across $\mathcal{I}$, is embedded in the variational formulation and can be recovered by integration by parts.
(ii) $\mathbf{A}$ and $\mathbf{curl}\,\mathbf{A}$ in $L^2(\tilde{\Omega})^3$, therefore

$$\int_{\tilde{\Omega}}|A_\varphi|^2 r\,dr\,dz\,d\varphi=2\,\pi\int_{\Omega}|A_\varphi|^2 r\,dr\,dz=2\,\pi\int_{\Omega}|\psi|^2\frac{1}{r}dr\,dz<\infty$$

and $\int_{\tilde{\Omega}}|\mathbf{curl}\,\mathbf{A}|^2 r\,dr\,dz\,d\varphi<\infty$ that is

$$2\,\pi\int_{\Omega}\frac{1}{r^2}|\nabla\,(r\,A_\varphi)|^2 r\,dr\,dz=2\,\pi\int_{\Omega}|\nabla\,\psi|^2\frac{1}{r}\,dr\,dz<\infty.$$

We thus remark that $\mathbf{A}\in H(\mathbf{curl},\tilde{\Omega})$ if and only if $\psi\in\mathcal{H}^1(\Omega)$ where

$$L^2_*(\Omega)=\{g:\Omega\to\mathbb{R},\quad \|g\|^2_{*,\Omega}:=\int_{\Omega}g^2\frac{1}{r}\,dr\,dz<\infty\}$$

and $\mathcal{H}^1(\Omega)=\{u\in L^2_*(\Omega),\ \nabla\,u\in L^2_*(\Omega)^2\}$ is the Hilbert space endowed with the norm $\|u\|^2_{\mathcal{H}^1(\Omega)}=\|u\|^2_{*,\Omega}+|u|^2_{\mathcal{H}^1(\Omega)}$ being $|u|^2_{\mathcal{H}^1(\Omega)}=\|\partial_r u\|^2_{*,\Omega}+\|\partial_z u\|^2_{*,\Omega}$. For $\psi\in\mathcal{H}^1(\Omega)$ the trace on γ_0 vanishes in the following sense [21]

$$\lim_{r\to 0^+}\int_{\{r\}\times[-\rho_\gamma,\rho_\gamma]\cap\Omega}\psi(r,z)^2\frac{1}{r^2}\,dz=0\,.$$

To formulate (2) (see Figure 2 (left)) as a variational problem in a non-overlapping domain decomposition framework, we set $\Omega=\Omega^{\rm in}\cup\Omega^{\rm ex}$ where $\Omega^{\rm in}$ is a bounded domain containing $\Omega_{\rm L}$ (see Figure 2 (right)) and $\Omega^{\rm ex}$ is the complement of $\Omega^{\rm in}$ in Ω (see Figure 2 (center)). The boundary of $\Omega^{\rm in}$ is denoted $\mathcal{I}$, to recall that it is an interface between the two subdomains $\Omega^{\rm in}$, $\Omega^{\rm ex}$, on which we will impose, at the discrete level, the continuity of ψ, in a weak sense, that is through a mortar-like L^2 projection [3]. Note that $\mathcal{I}=\overline{\Omega}^{\rm ex}\cap\overline{\Omega}^{\rm in}$. Let us now introduce the functional space $\mathcal{V}=\{(v,w)\in\mathcal{H}^1(\Omega^{\rm ex})\times\mathcal{H}^1(\Omega^{\rm in}),\ v_{|\gamma_0}=0,\ v_{|\mathcal{I}}=w_{|\mathcal{I}}\}$. Continuity is required for ψ in $\Omega^{\rm in}$ in order to have meaningful ψ_a and ψ_b that appear in the definition of $\Omega_{\rm p}$ and $\psi_{\rm N}$ [7, Remark I.5, page 18]. The weak formulation of (2) is: Find $\psi=(\psi_{\rm ex},\psi_{\rm in})\in\mathcal{V}$ such that

$$a(\psi,s):=a_{\rm ex}(\psi_{\rm ex},v)+a_{\rm in}(\psi_{\rm in},w)=\ell(I,s)\quad\forall s=(v,w)\in\mathcal{V}_{0,\mathcal{I}}\tag{8}$$

where $\mathcal{V}_{0,\mathcal{I}}=\mathcal{H}^1_0(\Omega^{\rm ex})\times\mathcal{H}^1_{0,\mathcal{I}}(\Omega^{\rm in})$. In (8), we have set

$$\begin{aligned}a_{\rm ex}(\psi,v)&:=\int_{\Omega^{\rm ex}}\frac{1}{\mu\,r}\,\nabla\,\psi\cdot\nabla\,v\,drdz+\mathsf{c}(\psi,v),\\ a_{\rm in}(\psi,w)&:=\int_{\Omega^{\rm in}}\frac{1}{\mu_0 r}\,\nabla\,\psi\cdot\nabla\,w\,drdz-\,\mathsf{J}_{\rm p}(\psi,w)\,,\end{aligned}$$

where

$$\begin{aligned}\mathsf{J}_{\rm p}(\psi,w)&:=\int_{\Omega_{\rm p}(\psi)}\lambda\left(\frac{r}{r_0}\mathcal{A}(\psi_{\rm N})+\frac{r_0}{r}\mathcal{B}(\psi_{\rm N})\right)w\,drdz\,,\\ \ell(I,s)&:=\sum_{i=1}^{N_c}\frac{I_i}{|\Omega_{{\rm c}_i}|}\int_{\Omega_{{\rm c}_i}}(\chi_{\Omega^{\rm ex}}v+\chi_{\Omega^{\rm in}}w)\,drdz\,,\end{aligned}\tag{9}$$

with $\ell(I,s)$ containing the expression $\chi_{\Omega^{\rm ex}}v+\chi_{\Omega^{\rm in}}w$ to take into account the presence of coils in $\Omega^{\rm in}$ and $\Omega^{\rm ex}$ (here, χ_D is the characteristic function of a set D).

The bilinear form $\mathsf{c}(\cdot,\cdot)$ is defined as

$$\mathsf{c}(\psi,\xi) := \frac{1}{\mu_0}\int_\Gamma \psi(\mathbf{x})N(\mathbf{x})\xi(\mathbf{x})dS(\mathbf{x}) + \frac{1}{2\mu_0}\int_\Gamma\int_\Gamma (\psi(\mathbf{x})-\psi(\mathbf{y}))M(\mathbf{x},\mathbf{y})(\xi(\mathbf{x})-\xi(\mathbf{y}))\,dS(\mathbf{x})\,dS(\mathbf{y})\,, \tag{10}$$

and accounts for the boundary conditions at infinity [1], with $\mathbf{x}=(\mathbf{x}_r,\mathbf{x}_z)$, $\mathbf{y}=(\mathbf{y}_r,\mathbf{y}_z)$ and

$$M(\mathbf{x},\mathbf{y}) = \frac{k_{\mathbf{x},\mathbf{y}}}{2\pi(\mathbf{x}_r\mathbf{y}_r)^{\frac{3}{2}}}\left(\frac{2-k^2_{\mathbf{x},\mathbf{y}}}{2-2k^2_{\mathbf{x},\mathbf{y}}}E(k_{\mathbf{x},\mathbf{y}}) - K(k_{\mathbf{x},\mathbf{y}})\right)$$
$$N(\mathbf{x}) = \frac{1}{\mathbf{x}_r}\left(\frac{1}{\delta_+}+\frac{1}{\delta_-}-\frac{1}{\rho_\Gamma}\right) \text{ and } \delta_\pm = \sqrt{\mathbf{x}_r^2+(\rho_\Gamma\pm\mathbf{x}_z)^2}\,.$$

Here, K and E are the complete elliptic integrals of first and second kind, respectively, and

$$k_{\mathbf{x},\mathbf{y}} = \sqrt{\frac{4\mathbf{x}_r\mathbf{y}_r}{(\mathbf{x}_r+\mathbf{y}_r)^2+(\mathbf{x}_z-\mathbf{y}_z)^2}}\,.$$

We refer to [20, Chapter 2.4] for the details of the derivation. Rigorous existence and uniqueness assertion for the general case are still an open problem. See [33, 2, 7, 30] for some theoretical work related to such results.

4 Coupling different finite elements on non-overlapping meshes

In the domain containing the plasma, we wish to have a finite element approximation ψ_h for the poloidal flux ψ that is not only continuous but has also continuous gradient $\nabla\psi_h$. This is possible if we use the reduced or minimal Hsieh-Clough-Tocher (rHCT) finite element space on a triangular mesh over $\bar\Omega^{\text{in}}$. The rHCT triangular element is one of the simplest elements which provide continuous differentiability of the approximated solution ψ_h. For the definition of a rHCT finite element on a triangle we refer to [9], [8] and to [5] for more details on the basis functions' definition. This regularity is not necessary in the external domain therefore we couple rHCT finite elements in Ω^{in} with continuous piece-wise linear finite elements on a mesh of triangles of $\bar\Omega$. We thus introduce τ^{ex} (resp. τ^{in}) a mesh of triangles that covers $\bar\Omega^{\text{ex}}$ (resp. $\bar\Omega^{\text{in}}$). The two meshes τ^{ex}, τ^{in} are shape regular and quasi-uniform. They are supposed to match at the common interface $\mathcal{I}$, that is $(\tau^{\text{ex}})_{|\mathcal{I}} = (\tau^{\text{in}})_{|\mathcal{I}}$. We assume that $\mathcal{I}$ is a polygonal with nodes and edges in τ^{ex} (this is adopted to write the discrete equivalent of the matching condition at interface $\mathcal{I}$). We denote by h_{ex} (resp. h_{in}) the maximum element diameter in τ^{ex} (resp. τ^{in}) and set $h=\max(h_{\text{ex}},h_{\text{in}})$.

4.1 The finite element spaces

Now, let us introduce the finite element spaces, that we use in the simulations. Locally, on one triangle, they are triples $(T,\mathcal{P}_{loc}(T),\Sigma(T))$ where T denotes a triangle of the mesh, $\mathcal{P}_{loc}(T)$ the local space of functions defined on that triangle and $\Sigma(T)$ a set of unisolvent degrees of freedom for the functions in the local space (see [8]). The indices i, $i+1$, $i+2$, in Definition 2 below, take values $1,2,3$. When $i+1>3$ (resp. $i+2>3$), we replace it by $[(i+1) \mod 3]+1$ (resp. $[(i+2) \mod 3]+1$).

Definition 1 *Let us denote by $T=[V_1,V_2,V_3]$ the triangle of vertices V_1,V_2,V_3. The $\mathbb{P}_1$ Lagrange finite element associated with T is the triple $(T,\mathbb{P}_1(T),\Sigma_0(T))$ where $\Sigma_0(T)=\{\sigma_i : v\mapsto v(V_i)\}_{i=1,2,3}$*

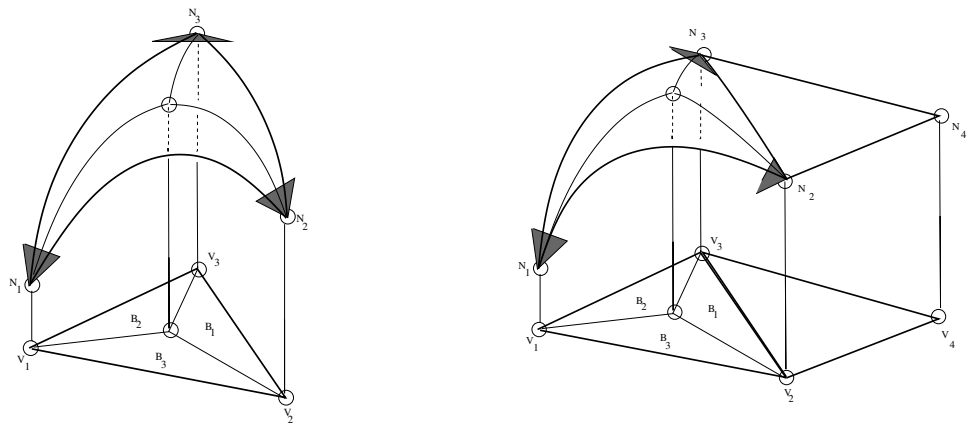

Figure 3: A visualization of the rHCT reconstruction of the function ψ in a triangle $T \in \tau^{\text{in}}$ (left). The mesh triangle $T = [V_1, V_2, V_3]$ is cut into three triangles $\mathtt{B}_i$: each $\mathtt{B}_i = [G, V_m, V_\ell]$ having vertices in V_m, V_ℓ with $m, \ell \in \{1, 2, 3\} \setminus \{i\}$ and at the barycenter G (denoted by the small circle at the interior) of the triangle T. We can thus reconstruct the height $N_i = \psi_h(V_i)$ of ψ at the three vertices V_i of T and the tangent plane to the surface ψ_h at the vertices V_i, as generated by $\partial_r \psi_h(V_i), \partial_z \psi_h(V_i)$. The coupling with a piece-wise linear element (right).

Definition 2 *Let us denote by $T = [V_1, V_2, V_3]$ the triangle of vertices V_1, V_2, V_3. The triangle T is divided into three subtriangles $\mathtt{B}_i = [G, V_{i+1}, V_{i+2}]$ where G is the barycenter of T (see Figure 3). The reduced Hsieh-Clough-Tocher (rHCT) finite element associated with T is the triple $(T, \mathcal{P}_{loc}(T), \Sigma(T))$, where $\mathcal{P}_{loc}(T)$ is the polynomial space of functions $w \in C^1(T)$ such that,*

$$w_{|\mathtt{B}_i} \in \mathbb{P}_3(\mathtt{B}_i) \quad \textit{and} \quad (\partial_n w)_{|\mathtt{b}_i} \in \mathbb{P}_1(\mathtt{b}_i) \quad \textit{for any edge } \mathtt{b}_i \in \partial \mathtt{B}_i \cap \partial T.$$

Here above, n is the outward normal vector to ∂T, $\mathtt{b}_i$ the edge on ∂T that does not insist in the vertex V_i and $(\partial_n w)_{|\mathtt{b}_i}$ the normal derivative of w at $\mathtt{b}_i$, and $\Sigma(T)$ is the set defined by the following functionals:

$$\zeta_{i,00} : w \mapsto w(V_i), \tag{11}$$

$$\zeta_{i,10} : w \mapsto (\mathbf{grad}\, w)(V_i) \cdot (V_{i+1} - V_i), \tag{12}$$

$$\zeta_{i,01} : w \mapsto (\mathbf{grad}\, w)(V_i) \cdot (V_{i+2} - V_i), \tag{13}$$

where $(\mathbf{grad} w)(V_i) \cdot (V_{i+1} - V_i)$ is the directional derivative of w on $[V_i, V_{i+1}]$. Note that $(\mathbf{grad}\, w)(V_i) \cdot (V_{i+1} - V_i) = (\partial_n w)_{|\mathtt{b}_{i+1}}(V_i) - (\partial_n w)_{|\mathtt{b}_i}(V_i)$.

Globally, over the meshes τ^{ex} and τ^{in}, the finite element spaces are, respectively,

$$\mathcal{V}^{\text{ex}} = \{v \in C^0(\Omega^{\text{ex}}),\, v_{|\gamma_0} = 0,\, v_{|T} \in \mathbb{P}_1(T),\, \forall\, T \in \tau^{\text{ex}}\}$$
$$\mathcal{V}^{\text{in}} = \{w \in C^1(\Omega^{\text{in}}),\, w_{|T} \in \mathcal{P}_{loc}(T),\, \forall\, T \in \tau^{\text{in}}\}$$

with the space $\mathcal{P}_{loc}(T)$ defined in Definition 2 . We then denote by $\mathcal{V}^{\text{ex}}_\partial$ (resp. $\mathcal{V}^{\text{in}}_\partial$) the trace space of $\mathcal{V}^{\text{ex}}$ (resp. $\mathcal{V}^{\text{in}}$) on the closed polygonal line $\mathcal{I}$. For functions in $\mathcal{V}^{\text{ex}}$, the degrees of freedom are given in Definition 1 . One degree of freedom is associated with each node $V_k \in \tau^{\text{ex}}$, so the total number of degrees of freedom in $\mathcal{V}^{\text{ex}}$ is equal to N^{ex}, the total number of mesh nodes in τ^{ex}, divided into N^{ex}_∂ nodes on the interface $\mathcal{I}$ and the remaining N^{ex}_o nodes on $\bar{\Omega}^{\text{ex}} \setminus \mathcal{I}$. For

functions $\mathcal{V}^{\rm in}$, the degrees of freedom are given in Definition 2. Three degrees of freedom are associated with each node $V_k \in \tau^{\rm in}$, so the total number of degrees of freedom in $\mathcal{V}^{\rm in}$ is equal to $3N^{\rm in}$, being $N^{\rm in} = N_o^{\rm in} + N_\partial^{\rm in}$ the total number of mesh nodes in $\tau^{\rm in}$ divided into $N_\partial^{\rm in}$ nodes on the interface $\mathcal{I}$ and the remaining $N_o^{\rm in}$ nodes on $\bar{\Omega}^{\rm in} \setminus \mathcal{I}$. By the definition of $\mathcal{V}^{\rm ex}$ and $\mathcal{V}^{\rm in}$ there are finite element spaces $\mathcal{V}_\circ^{\rm ex}$ and $\mathcal{V}_\circ^{\rm in}$ such that

$$\mathcal{V}^{\rm ex} = \mathcal{V}_\circ^{\rm ex} \oplus \mathcal{E}\mathcal{V}_\partial^{\rm ex} \quad \text{and} \quad \mathcal{V}^{\rm in} = \mathcal{V}_\circ^{\rm in} \oplus \mathcal{E}\mathcal{V}_\partial^{\rm in},$$

where $\mathcal{E}$ denotes the trivial extension operators. The elements of $\mathcal{V}_\circ^{\rm ex}$ and $\mathcal{V}_\circ^{\rm in}$ have vanishing Dirichlet trace on $\mathcal{I}$.

4.2 The discrete coupling condition

Let us denote by $\{v_i^{\rm ex}\}_{i=1,N^{\rm ex}}$ the basis of $\mathcal{V}^{\rm ex}$ in duality with the degrees of freedom of Definition 1 associated with vertices $V_i \in \tau^{\rm ex}$ and $\{w_j^{\rm in}\}_{j=1,3N^{\rm in}}$ that of $\mathcal{V}^{\rm in}$ in duality with the degrees of freedom of Definition 2 associated with vertices $V_j \in \tau^{\rm in}$. Then, if $\mathbf{u}^{\rm ex}$ and $\mathbf{u}^{\rm in}$ represent the vectors gathering the values of degrees of freedom of $\psi_h^{\rm ex} \in \mathcal{V}^{\rm ex}$ and $\psi_h^{\rm in} \in \mathcal{V}^{\rm in}$ we have the decomposition $\mathbf{u}^{\rm ex} = (\mathbf{u}_\circ^{\rm ex}, \mathbf{u}_\partial^{\rm ex})$ and $\mathbf{u}^{\rm in} = (\mathbf{u}_\circ^{\rm in}, \mathbf{u}_\partial^{\rm in})$ where $\mathbf{u}_\circ^{\rm ex}$ (resp. $\mathbf{u}_\circ^{\rm in}$) and $\mathbf{u}_\partial^{\rm ex}$ (resp. $\mathbf{u}_\partial^{\rm in}$) are the degrees of freedom in $V_\circ^{\rm ex}$ (resp. $V_\circ^{\rm in}$) and $V_\partial^{\rm ex}$ (resp. $V_\partial^{\rm in}$). Since the differential operator $-\Delta^*$ is only second order, there is no transmission condition on $(\partial_n \psi_h)_\mathcal{I}$ to be included in the discrete space [3]. Examples of MEM coupling between rHCT FEs on both subdomains can be found to solve problems involving four-order operators (we refer to [29] for convergence studies with application to elasticity). In plasma physics, the requirement of $\mathcal{C}^1$ continuity all over Ω could be necessary when discretizing, for example, reduced MHD models which are characterised by stream function formulations and thus require a proper discretization of four-order operators (see [6]).

4.2.1 The interpolation case

The imposition of the transmission condition $[\psi_h]_\mathcal{I} = 0$ by interpolation means to ask for the equality

$$(\psi_h^{\rm ex})_{|\mathcal{I}}(V) = \sum_{j=1}^{N_\partial^{\rm ex}} (\mathbf{u}_\partial^{\rm ex})_j \, v_j^{\rm ex}(V) = \sum_{k=1}^{N_\partial^{\rm in}} (\mathbf{u}_\partial^{\rm in})_k \, w_k^{\rm in}(V) = (\psi_h^{\rm in})_{|\mathcal{I}}(V)\,, \qquad \forall\, V \in \mathcal{I}. \tag{14}$$

If the meshes $\tau^{\rm ex}$, $\tau^{\rm in}$ are coincident at $\mathcal{I}$, then (14) becomes $\mathbf{u}_\partial^{\rm ex} = \mathbf{u}_\partial^{\rm in}$. If the meshes $\tau^{\rm ex}$, $\tau^{\rm in}$ were not coincident at $\mathcal{I}$, relation (14) for $V \equiv V_i \in (\tau^{\rm ex})_{|\mathcal{I}}$ would read $\mathbf{P}\,\mathbf{u}_\partial^{\rm ex} = \mathbf{D}\,\mathbf{u}_\partial^{\rm in}$ where

$$\begin{aligned} (\mathbf{P})_{ij} &= v_j^{\rm ex}(V_i) = \delta_{ij}, \quad i,j = 1, N_\partial^{\rm ex} \\ (\mathbf{D})_{i,k} &= w_k^{\rm in}(V_i), \qquad i = 1, N_\partial^{\rm ex}, \qquad k = 1, N_\partial^{\rm in}. \end{aligned}$$

By looking at Figure 4, we remark that relation (14) allows to pass the information on the values of ψ_h at the interface $\mathcal{I}$ (left-hand side of the figure) without influencing the value of $\partial_n \psi_h$ (right-hand side of the figure). Indeed, with matching grids and a point-wise coupling, the block contained in $\mathbf{u}_\partial^{\rm in}$ and associated with the degrees of freedom (12), (13) of Definition 2 at $V_i \in \mathcal{I}$ is not involved to define $\mathbf{u}_\partial^{\rm ex}$.

4.2.2 The L^2-projection case

The imposition of the transmission condition $[\psi_h]_\mathcal{I} = 0$ in a weak sense, by mortar L^2-projection, means to ask that

$$\int_{\mathcal{I}_h} u_h^{\rm ex} \, z_h \, d\mathcal{I} = \int_{\mathcal{I}_h} u_h^{\rm in} \, z_h \, d\mathcal{I}, \qquad \forall\, z_h \in \mathcal{M}_h \tag{15}$$

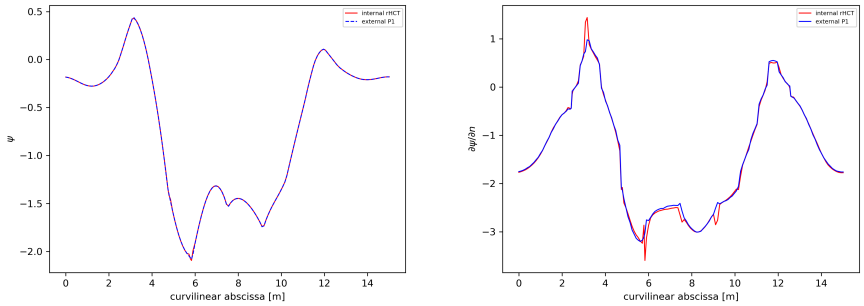

Figure 4: The profile of ψ_h (left) and $\partial_n \psi_h$ (right) at the interface edge mid-points, with pointwise interpolation on matching grids.

where $\mathcal{I}_h$ denotes the description of the interface in terms of edges of the *slave* side mesh (this will become clear with the definition of $\mathcal{M}_h$) and $\mathcal{M}_h$ is a space of Lagrange multipliers, the choice of which is of crucial importance in the error analysis. For simplicity, we omit the foot-index h on $\mathcal{I}$ (also because we consider matching grids at the common interface). The mathematical rationale behind the imposition of the transmission condition by L^2-projection (rather than the more natural condition of pointwise continuity (14) at a chosen set of grid nodes on $\mathcal{I}$) becomes clear from the convergence analysis, shortly presented in Remark 2. This type of condition was firstly studied by Bernardi, Maday and Patera [3], who introduced the mortar element method (MEM) to generalize the spectral element method to geometrically nonconforming partitions, to subdomains with different resolutions (polynomial degrees) on subdomain interfaces, and also to allow the coupling of spectral element methods with other methods, such as, *e.g.*, the h-version of the finite element method. Its generality and flexibility go far beyond these two specific examples (see [4]).

Here, we define the mortar multiplier space as $\mathcal{M}_h = \{\xi_h \in \mathcal{C}^0(\mathcal{I}) \,:\, \xi_{h|e} \in \mathbb{P}_1(e)\,, \forall\, e \in (\tau^{\rm ex})_{|\mathcal{I}}\}$. It coincides with the whole trace space $\mathcal{V}_\partial^{\rm ex}$, due to the fact that $\mathcal{I}$ is a closed curve. In the mortar terminology, the choice of $\mathcal{M}_h$ confers to $\Omega^{\rm in}$ the master role (resp. to $\Omega^{\rm ex}$ the slave role) with respect to passing the information (value of ψ_h) across $\mathcal{I}$. The left-hand-side of (15) raises no difficulty to be computed since the two discrete functions $u_h^{\rm ex}$, z_h live on the same mesh inherited from $\tilde{\Omega}^{\rm ex}$ on $\mathcal{I}$. On the contrary, the right-hand-side involves discrete functions that live on different meshes. Whenever the meshes $\tau^{\rm ex}$, $\tau^{\rm in}$ coincide or not at $\mathcal{I}$, to compute efficiently the integrals in the coupling condition we rely on numerical quadrature. Relation (15) links the block $\mathbf{u}_\partial^{\rm ex}$ to the block $\mathbf{u}_\partial^{\rm in}$ by the matrix relation $\mathbf{P}\,\mathbf{u}_\partial^{\rm ex} = \mathbf{D}\,\mathbf{u}_\partial^{\rm in}$ where this time

$$
\begin{aligned}
(\mathbf{P})_{i,j} &= \textstyle\int_{\mathcal{I}} v_{\partial,i}^{\rm ex}\, v_{\partial,j}^{\rm ex}\, dr\, dz \qquad && i,j = 1, N_\partial^{\rm ex}\,,\\
(\mathbf{D})_{i,k} &= \textstyle\int_{\mathcal{I}} v_{\partial,i}^{\rm ex}\, w_{\partial,k}^{\rm in}\, dr\, dz \qquad && i = 1, N_\partial^{\rm ex},\ k = 1, N_\partial^{\rm in}\,,
\end{aligned}
$$

with $\mathcal{I}$ represented in $\tau^{\rm ex}$. Locally, on each edge $e \in \mathcal{I}$, the 2 entries of the block $\mathbf{u}_\partial^{\rm ex}$ are defined in terms of the 6 entries of the block $\mathbf{u}_\partial^{\rm in}$.

By looking at Figure 5, we can see that relation (15) allows to pass the information on the values of ψ_h at the interface $\mathcal{I}$ (left-hand side of the figure) improving the behavior of $\partial_n \psi_h$ (right-hand side of the figure). Indeed, with the relation (15), the block $\mathbf{u}_\partial^{\rm in}$ is now completely involved in defining $\mathbf{u}_\partial^{\rm ex}$. We recall that there is no condition imposed on $[\partial_n \psi_h]_{|\mathcal{I}}$, however a good behavior of $\partial_n \psi_h$ passing through the interface $\mathcal{I}$ is important to keep under control the consistency error (as explained later in Remark 2). The behavior of $\partial_n \psi_h$ at the interface $\mathcal{I}$ cannot be improved further by considering for example quadratic multipliers. According to

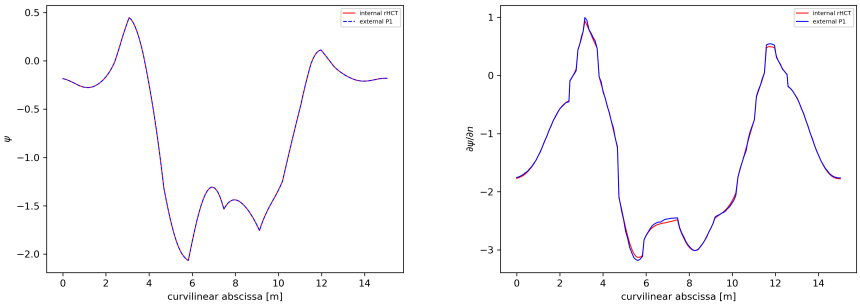

Figure 5: The profile of ψ_h (left) and $\partial_n \psi_h$ (right) at the interface edge mid-points, with mortar L^2-projection by linear mutipliers.

Definition 2, we have $(\partial_n \psi_h^{\text{in}})_{|e} \in \mathbb{P}_1(e)$, for all edges for all $e \in \mathcal{I}$.

Remark 1 *In order to confer to Ω^{ex} the master role (resp. to Ω^{in} the slave role) with respect to passing the information (value of ψ_h) across the interface $\mathcal{I}$, in the coupling condition (15), we have to select the space $\mathcal{M}_h = \{\xi_h \in \mathcal{C}^1(\mathcal{I}) \,:\, \xi_{h|e} \in \mathbb{P}_3(e)\,, \forall\, e \in (\tau^{\text{in}})_{|\mathcal{I}}\}$. With this choice, locally, on each edge $e \in \mathcal{I}$, the 6 entries of the block $\mathbf{u}_\partial^{\text{in}}$ would be defined in terms of the 2 entries of the block $\mathbf{u}_\partial^{\text{ex}}$.*

4.2.3 The discrete problem

We set $\mathcal{X}_h = \{u_h \in L^2(\Omega) \,:\, u_{h|\Omega^{\text{in}}} = u_h^{\text{in}} \in \mathcal{V}^{\text{in}}\,,\, u_{h|\Omega^{\text{ex}}} = u_h^{\text{ex}} \in \mathcal{V}^{\text{ex}}\}$, where $h = \max(h_{\text{ex}}, h_{\text{in}})$ and the discrete space

$$\mathcal{V}_h = \{u_h \in \mathcal{X}_h \,:\, u_{h|\gamma_0}^{\text{ex}} = 0 \;\text{ and }\; (15)\,\}. \tag{16}$$

The discrete problem to solve reads: Find $\psi_h \in \mathcal{V}_h$ such that

$$a(\psi_h, s_h) = \ell(\vec{I}, s_h) \quad \forall s_h = (v_h, w_h) \in \mathcal{V}_\circ^{\text{ex}} \times \mathcal{V}_\circ^{\text{in}}. \tag{17}$$

The bilinear and linear forms $a(.,.)$, $\ell(\vec{I},.)$ are defined as for the problem (8) and evaluated in (17) for the functions in the discrete space.

Remark 2 *The presence of the weak coupling condition (15) prevents $\mathcal{V}_h$ from being a subspace of $\mathcal{V}$,* i.e.*, we are using a non-conforming method to approximate the solution of the problem (8). The second Strang lemma allows to derive the following error bound for such an approximation*

$$||u - u_h||_{1,*} \leq c \left\{ \inf_{z_h \in \mathcal{V}_h} ||u - z_h||_{1,*} + \sup_{z_h \in \mathcal{V}_h} \frac{\int_{\mathcal{I}} \partial_n u\, [z_h]_{\mathcal{I}} d\mathcal{I}}{||z_h||_{1,*}} \right\} \tag{18}$$

where $||.||_{1,*}$ is the broken norm $||z_h||_{1,*}^2 = ||z_h^{\text{ex}}||_{1,\Omega^{\text{ex}}}^2 + ||z_h^{\text{in}}||_{1,\Omega^{\text{in}}}^2$. In the right-hand side of (18), the first term represents the best approximation error of ψ (that is, the distance between the exact solution ψ and the finite-dimensional space $\mathcal{V}_h$) and the extra error, the second, involving interface jumps, is known as the consistency error. The consistency error is related to the "variational crime" on the conformity property, due to the fact of dealing with a discrete space $\mathcal{V}_h \not\subset \mathcal{V}$. The error estimate (18) is optimal if each term on the right-hand side can be bounded by the norm of local errors arising from the approximation of ψ in Ω^{ex} and Ω^{in}, in an additive fashion. In this way, we can take advantage of the local regularity of the exact solution as well as

the approximation properties enjoyed by the local subspaces. The second term is optimal owing to the special choice of the mortar. In fact, due to the orthogonality property (15), we can subtract from $\partial_n\psi$ an arbitrary function $z_h \in \mathcal{M}_h$. It is therefore important that such functions allow for an optimal approximation of the normal derivative of ψ at the interface. In the present cas, with the choice we made, we have both $\partial_n\psi_h^{\rm in} \in \mathbb{P}_1(\mathcal{I})$ and $\mathcal{M}_h = \mathbb{P}_1(\mathcal{I})$, with $\mathcal{I}$ described in the same way by $\tau^{\rm ex}$ and $\tau^{\rm in}$.

5 The discrete problem in matrix form

Let us first focus on the discrete problem in $\Omega^{\rm in}$, that reads : Find $\psi_h \in \mathcal{V}^{\rm in}$, with $\psi_h = g_D$ on $\mathcal{I}$, such that

$$\int_{\Omega^{\rm in}} \frac{1}{\mu_0 r}\nabla\psi_h\cdot\nabla w_h\, dr\, dz - \int_{\Omega_{\rm p}(\psi_h)} {\rm J}_\varphi(\psi_{{\rm N},h}, r)\, w_h\, dr\, dz = \sum_{\Omega_{{\rm c}_i}\subset\Omega^{\rm in}} \frac{I_i}{|\Omega_{{\rm c}_i}|}\int_{\Omega_{{\rm c}_i}} w_h\, drdz\,, \qquad \forall w_h \in \mathcal{V}_\circ^{\rm in}, \tag{19}$$

with ${\rm J}_\varphi(\psi_{\rm N}, r) = \lambda(\frac{r}{r_0}\mathcal{A}(\psi_{\rm N}) + \frac{r_0}{r}\mathcal{B}(\psi_{\rm N}))$ and g_D is a given function representing a Dirichlet data. With $N^{\rm in} = N_\circ^{\rm in} + N_\partial^{\rm in}$, the space $\mathcal{V}^{\rm in}$ (resp. $\mathcal{V}_\circ^{\rm in}$) has dimension $n = 2N^{\rm in} + N_\circ^{\rm in}$ (resp. $3N^{\rm in} = n + N_\partial^{\rm in}$). At a point $(r,z) \in \Omega^{\rm in}$, we have

$$\psi_h(r,z) = \sum_{j=1}^{n} \psi_j\, w_j(r,z) + \sum_{\ell=1}^{N_\partial^{\rm in}} g_{D,\ell}\, v_{D,\ell}(r,z),$$

where $\{w_j\}_j$ (resp., $\{\psi_j\}_j$) is the set of n basis functions (resp., n degrees of freedom) for the rHCT finite element space $\mathcal{V}_\circ^{\rm in}$ and $\{v_{D,\ell}\}_\ell$ the set of $N_\partial^{\rm in}$ basis functions for rHCT finite elements associated with the values of the discrete function at the mesh boundary nodes of $\mathcal{I}$. The reals $\{g_{D,\ell}\}_\ell$ are the values of the Dirichlet boundary condition at the mesh nodes on $\mathcal{I}$. The normalized discrete flux is $\psi_{{\rm N},h}(r,z) = (\psi_N(\psi_h(r,z)), \psi_a(\psi_h), \psi_b(\psi_h))$ with

$$\psi_a(\psi_h) = \psi_h(r_a, z_a), \qquad \psi_b(\psi_h) = \psi_h(r_b, z_b). \tag{20}$$

The critical points (r_a, z_a) and (r_b, z_b) are not necessarily located at nodes of the mesh, as is the case with piece-wise linear finite elements, and in this work we use a Newton method to find them by solving $\nabla\psi_h(r,z) = 0$.

We use a six-point quadrature rule of order 4 (see [28]) on each sub-triangle for the approximation of integrals in (19). A difficulty which arises with rHCT finite elements is the computation of the iso-contours and therefore of the plasma boundary $\Gamma_p(\psi_h)$. Contrary to what has been done in [22, 12] with piece-wise linear finite elements, we do not compute explicitely the plasma boundary and do not consider a specific quadrature rule for elements T such that the intersection $T \cap \Omega_{\rm p}(\psi_h)$ is neither empty nor the whole triangle. We do not look for such elements T, but rather set $\mathcal{A}(\psi_{{\rm N},h}(r,z)) = 0$ and $\mathcal{B}(\psi_{{\rm N},h}(r,z)) = 0$ for points (r,z) outside the plasma domain. Once (r_b, z_b) and (r_a, z_a) are known, the plasma domain can be defined as $\{(r,z) \in \Omega, 0 \le \psi_{{\rm N},h}(r,z) \le 1$ and $\nabla\psi_h(r,z)\cdot(r_a - r, z_a - z)^\top \ge 0\}$. The integral of the current density term over the plasma domain is then approximated with the same quadrature rule as for the linear term.

Let us denote by $\boldsymbol{\psi}$ the vector gathering the n degrees of freedom $\{\psi_i\}_i$ and $\mathbf{g}_D$ the vector of size $N_\partial^{\rm in}$ collecting the values of the Dirichlet boundary conditions. The first term in (19) leads to the linear expression $\boldsymbol{A}\boldsymbol{\psi} + \boldsymbol{A}_D\mathbf{g}_D$, where $\boldsymbol{A}$ is the $n\times n$ stiffnes matrix and $\boldsymbol{A}_D$ is the $n \times N_\partial^{\rm in}$

matrix associated with the boundary conditions. The second term leads to the definition of a vector $\mathbf{J}(\boldsymbol{\psi})$ of size n with components

$$(\mathbf{J}(\boldsymbol{\psi}))_i = \int_{\Omega_{\mathrm{p}}(\psi_h)} \mathrm{J}_\varphi(\psi_{\mathrm{N},h}, r)\, w_i \, dr\, dz, \qquad i = 1, n, \tag{21}$$

that depend non-linearly on $\boldsymbol{\psi}$. Using the quadrature method explained above and denoting by T_i the subset of elements T of τ_{in} to which the node of the mesh associated with the ith degree of freedom belongs, and by $\mathbf{x}_{q,T} = (r_{q,T}, z_{q,T})$, $\omega_{q,T}$, the quadrature points and weights in the element T, the integral is computed as

$$\mathbf{J}(\boldsymbol{\psi})_i = \sum_{T\in T_i} \sum_q \mathrm{J}_\varphi(\psi_{\mathrm{N},h}(\mathbf{x}_{q,T}), r_{q,T})\, w_i(\mathbf{x}_{q,T})\, \omega_{q,T}. \tag{22}$$

In order to derive a Newton's method, we need to compute the Jacobian matrix $\mathbf{Jac}_{\boldsymbol{\psi}}(\boldsymbol{\psi})$ which follows from the chain rule now that all notations are set:

$$\begin{aligned}
[\mathbf{Jac}_{\boldsymbol{\psi}}(\boldsymbol{\psi})]_{ij} &= \sum_{T\in T_i} \sum_q \omega_{q,T}\, w_i(\mathbf{x}_{q,T})\, \frac{\partial \mathrm{J}_\varphi}{\partial \psi_{\mathrm{N}}}(\psi_{\mathrm{N},h}(\mathbf{x}_{q,T}), r_{q,T})\, [\frac{\partial \psi_{\mathrm{N}}}{\partial \psi}\frac{\partial \psi_h}{\partial \psi_j} + \frac{\partial \psi_{\mathrm{N}}}{\partial \psi_a}\frac{\partial \psi_a}{\partial \psi_j}(\psi_h) + \frac{\partial \psi_{\mathrm{N}}}{\partial \psi_b}\frac{\partial \psi_b}{\partial \psi_j}(\psi_h)] \\
&= \sum_{T\in T_i} \sum_q \omega_{q,T}\, w_i(\mathbf{x}_{q,T})\, \frac{\partial \mathrm{J}_\varphi}{\partial \psi_{\mathrm{N}}}(\psi_{\mathrm{N},h}(\mathbf{x}_{q,T}), r_{q,T})\, \frac{1}{(\psi_b - \psi_a)}\, [w_j(\mathbf{x}_{q,T}) + \frac{\psi_h(\mathbf{x}_{q,T}) - \psi_b}{(\psi_b - \psi_a)} w_j(\mathbf{x}_a) \\
&\qquad - \frac{\psi_h(\mathbf{x}_{q,T}) - \psi_a}{(\psi_b - \psi_a)} w_j(\mathbf{x}_b)]
\end{aligned} \tag{23}$$

where $w_j(\mathbf{x}_a)$ (resp. $w_j(\mathbf{x}_b)$) are null for indices j not corresponding to the element T_a (resp., T_b) where $\mathbf{x}_a = (r_a, z_a)$ (resp., $\mathbf{x}_b = (r_b, z_b)$) lies. Nevertheless $\mathbf{Jac}_{\psi}(\boldsymbol{\psi})$ has entries at indices (i, j) not local to an element. Each element T is linked to T_a (resp. T_b) through the $w_i(\mathbf{x}_{q,T})w_j(\mathbf{x}_a)$ (resp. $w_i(\mathbf{x}_{q,T})w_j(\mathbf{x}_b)$) terms. This is not standard but the matrix can still be assembled element by element as it is usually done with finite elements. For the right-hand-side of equation (19), we introduce the matrix $\mathbf{L}^{\mathrm{in}}$ of size $n \times N_c^{\mathrm{in}}$ with entries

$$\mathbf{L}^{\mathrm{in}}_{i,j} = \frac{1}{|\Omega_{\mathrm{c}_i}|} \int_{\Omega_{\mathrm{c}_i}} w_j^{\mathrm{in}}\, dr\, dz, \qquad \Omega_{\mathrm{c}_i} \subset \Omega^{\mathrm{in}},$$

and the vector $\mathbf{U}_I^{\mathrm{in}}$ of size N_c^{in} holding the currents I_i of the coils $\Omega_{\mathrm{c}_i} \subset \Omega^{\mathrm{in}}$. Newton's iterations for equation (19) in its fully discretized form, say $\mathbf{e}(\boldsymbol{\psi}) = \mathbf{0}$ with $\mathbf{e}(\boldsymbol{\psi}) := \boldsymbol{A}\boldsymbol{\psi} + \boldsymbol{A}_D\mathbf{g}_D - \mathbf{J}(\boldsymbol{\psi}) - \mathbf{L}^{\mathrm{in}}\,\mathbf{U}_I^{\mathrm{in}}$, can be written as

$$\boldsymbol{\psi}^{k+1} = \boldsymbol{\psi}^k - [\mathbf{e}_{\boldsymbol{\psi}}(\boldsymbol{\psi}^k)]^{-1}\,\mathbf{e}(\boldsymbol{\psi}^k), \qquad [\mathbf{e}_{\boldsymbol{\psi}}(\boldsymbol{\psi})] = \boldsymbol{A} - \mathbf{Jac}_{\boldsymbol{\psi}}(\boldsymbol{\psi})\,. \tag{24}$$

In order to write the matrix form of the discrete problem in the whole domain, instead of a Dirichlet type datum $\mathbf{g}_D$ on the boundary $\mathcal{I}$, we have to impose the mortar coupling condition. We denote by $\mathbf{X}$ the reduced variable such that $\boldsymbol{\psi} = \mathbf{Q}\,\mathbf{X}$ with $\mathbf{Q}$ the coupling matrix. In detail, we have

$$\boldsymbol{\psi} = \begin{pmatrix} \mathbf{u}_\circ^{\mathrm{ex}} \\ \mathbf{u}_\partial^{\mathrm{ex}} \\ \mathbf{u}_\circ^{\mathrm{in}} \\ \mathbf{u}_\partial^{\mathrm{in}} \end{pmatrix} = \begin{bmatrix} I & 0 & 0 \\ 0 & 0 & \mathbf{P}^{-1}\mathbf{D} \\ 0 & I & 0 \\ 0 & 0 & I \end{bmatrix} \begin{pmatrix} \mathbf{u}_\circ^{\mathrm{ex}} \\ \mathbf{u}_\circ^{\mathrm{in}} \\ \mathbf{u}_\partial^{\mathrm{in}} \end{pmatrix} = \mathbf{Q}\,\mathbf{X},$$

with the matrices $\mathbf{P}$ and $\mathbf{D}$ defined in the previous section. So, $\mathbf{J}(\boldsymbol{\psi}) = \mathbf{J}(\mathbf{Q}\,\mathbf{X}) = \mathbf{H}(\mathbf{X})$ and when we derive $\mathbf{J}(\boldsymbol{\psi})$ with respect to $\mathbf{X}$ we have $D_{\mathbf{X}}\mathbf{H}(\mathbf{X})d\mathbf{X} = \mathbf{Jac}_{\boldsymbol{\psi}}(\boldsymbol{\psi})\mathbf{Q}d\mathbf{X}$. Newton's

iterations for problem (8) in its fully discretized form, say $\mathbf{e}(\mathbf{X}) = \mathbf{0}$ with now $\mathbf{e}(\mathbf{X}) := \mathbf{Q}^\top\,[(\boldsymbol{A}+\mathbf{C})\,\mathbf{Q}\,\mathbf{X} - \mathbf{J}(\boldsymbol{\psi}) - \mathbf{L}\,\mathbf{U}_I]$, can be written as

$$\mathbf{X}^{k+1} = \mathbf{X}^k - [\mathbf{e}_\mathbf{X}(\mathbf{X}^\mathbf{k})]^{-\mathbf{1}}\,\mathbf{e}(\mathbf{X}^\mathbf{k}), \qquad [\mathbf{e}_\mathbf{X}(\mathbf{X})] = \mathbf{Q}^\top[(\boldsymbol{A}+\mathbf{C}) - \mathbf{Jac}_{\boldsymbol{\psi}}(\boldsymbol{\psi}^\mathbf{k})]\,\mathbf{Q}\,. \tag{25}$$

Here, $\mathbf{L}$ (resp. $\mathbf{U}_I$) now takes into account the contributions associated with all the coils (resp. all the currents I_i of the coils) contained in Ω^{in} and in Ω^{ex}. See the section on numerical results for a convergence history of the proposed Newton's method.

6 Computation of geometric coefficients

Important outputs of an equilibrium computation are 1D profiles computed from integrals of the form

$$A_{\alpha,\beta}(y) = \int_{C_y} r^\alpha |\nabla\psi_h|^\beta ds \tag{26}$$

defined on iso-contours $C_y = \{\mathbf{x} \in \Omega_\text{p},\ \psi_\text{N}(\mathbf{x}) = y\}$, for $y \in [0,1]$, in the plasma domain. Note that the iso-contour C_y is a priori not given by an explicit parametrization, but implicitly as level set of a scalar function. The 1D profiles, such as (26), are essential to incorporate resistive diffusion effects into plasma evolution modeling. Also many plasma characteristics (*e.g.*, the safety factor or the averaged current density profile), that are important to quantify stability or for monitoring during the experiment, are defined as integrals over iso-contours [6]. These 1D profiles are used for example in the definition of averaged quantities

$$< r^\alpha |\nabla\psi_h|^\beta >= \frac{A_{\alpha+1,\beta-1}}{A_{1,-1}}.$$

With $\mathbb{P}_1$ Lagrange FE, high accuracy in computing these profiles can be achieved only by relying on a very fine mesh. The use of rHCT FEs enables to compute a smooth poloidal magnetic field and to locate precisely the position of the magnetic axis and of the X-point independently of the mesh. At a fixed number of degrees of freedom, it improves the precision of the computation of these 1D profiles with respect to that with $\mathbb{P}_1$ Lagrange FEs.

6.1 The iso-contour method

A drawback of using rHCT FE is that the computation of precise iso-contours for ψ is much more involved than when using $\mathbb{P}_1$ Lagrange FEs. Nevertheless, it is possible and we can proceed as follows: Given the magnetic axis and the point defining the plasma boundary, iterate, until convergence (up to a fixed threshold), the following steps.

1. Find a first point $\mathbf{x}_y^0$ on the levelset C_y, where $\psi_y := \psi_a + (\psi_b - \psi_a)y$ thanks to a Newton's method along the ray $(\mathbf{x}_a, \mathbf{x}_b)$.
2. Construct isocontour points by first following the direction $\mathbf{t}$ orthogonal to $\nabla\psi_h$ with a step a, namely, set $\mathbf{x}_y^{k+1,0} = \mathbf{x}_y^k + a\mathbf{t}$.
3. Correct $\mathbf{x}_y^{k+1,0}$ to obtain a point located exactly on the levelset, with iterations

$$\mathbf{x}_y^{k+1,\ell+1} = \mathbf{x}_y^{k+1,\ell} + \delta s\, \nabla\psi_h(\mathbf{x}_y^{k+1,\ell})$$

where δs is the Newton's increment for $\psi_h(\mathbf{x}_y^{k+1,\ell} + s\,\nabla\psi_h(\mathbf{x}_y^{k+1,\ell})) - \psi_y = 0$.
If $||\mathbf{x}_y^{k+1,\ell+1} - \mathbf{x}_y^{k+1,\ell}||_2$ inferior to a fixed threshold ε, stop and proceed with next point, otherwise go back to step 2 and reduce step size a.

Typically in our numerical tests (see Section 7) the step a is set to a fraction of h_{in}, $a = \frac{h_{in}}{4}$, the threshold is $\varepsilon = 10^{-12}$ and the Newton loop in step 3 above converges in 2 iterations.

Once the levelset points are found, the integrals (26) are computed using the trapezoidal quadrature rule. This method works perfectly well and gives precise results but the computation of iso-contours can be time consuming. On the other hand these computations are completely independent one from the other and can thus be easily parallelized.

6.2 The weak formulation method

In [10] it is proposed to use a weak formulation based on the coarea formula (see Theorem 3.2.12 in [14]) to compute integrals such as (26). The coarea formula underlines the relationship between integrals on iso-contours and integrals on $\Omega \subset \mathbb{R}^d$, here $d = 2$. Given a function $f : \Omega \to \bar{\mathbb{R}}$ integrable and $\psi_N : \Omega \to [0,1]$ Lipschitz continuous, the iso-contour integrals are defined as $g_{f,\psi_N}(y) := \int_{\mathbf{x}\in\Omega,\, \psi_N(\mathbf{x})=y} f(\mathbf{x})\, d\mathbf{x}$. The coarea formula states that $g_{f,\psi_N} \in L^1(0,1)$ and

$$\int_0^1 g_{f,\psi_N}(y)\, dy = \int_\Omega f(\mathbf{x})\, |\nabla\psi_N(\mathbf{x})|\, d\mathbf{x}. \tag{27}$$

As done in [10], from the identity $g_{f,\psi_N}(y)\,\lambda(y) = g_{f\,\lambda(\psi_N),\psi_N}(y)$ and (27), we have

$$\int_0^1 g_{f,\psi_N}(y)\,\lambda(y)\, dy = \int_0^1 g_{f\,\lambda(\psi_N),\psi_N}(y)\, dy = \int_\Omega f(\mathbf{x})\,\lambda(\psi_N(\mathbf{x}))\, |\nabla\psi_N(\mathbf{x})|\, d\mathbf{x}. \tag{28}$$

By combining (28) and (26), we have :

$$\int_0^1 A_{\alpha,\beta}(y)\lambda(y)dy = \int_{\Omega_{\mathrm{p}}(\psi_h)} r^\alpha |\nabla\psi_h|^\beta \lambda(\psi_{\mathrm{N},h})|\nabla\psi_{\mathrm{N},h}| dr dz, \quad \forall\lambda \in L^2(0,1) \tag{29}$$

In [10], to approximate $L^2(0,1)$, the space of all polynomials of degree less than or equal to P in $[0,1]$ is used as discrete space, with a basis of Legendre polynomials. This enables to have a diagonal $(P+1)\times(P+1)$ mass matrix corresponding to the left-hand side of (29) but on the other hand requires the use of an expensive high order quadrature formula to compute terms corresponding to the right-hand side of (29) since Legendre polynomials up to degree 30 or 40 have to be used. In this paper we have succesfully tested the use of a cubic spline basis which does not require such high order quadrature formulas.

We propose an equivalent formulation of (26) which does not involve anymore the explicit computation of iso-contours. Numerically the method consists in writing $A_{\alpha,\beta}(y) = \sum_i a^i_{\alpha,\beta}\lambda_i(y)$,

Table 1: Error values in $H^m(\Omega^{\text{in}})$-norm, $m = 0, 1, 2$, for the linear problem (30) using rHCT FEs on refined meshes.

h	$\|\|u - u_h\|\|_{L^2}$	$\|\|u - u_h\|\|_{H^1}$	$\|\|u - u_h\|\|_{H^2}$
0.44194174e-1	0.99885478e-5	0.15105871e-2	0.33870552e-0
0.22097087e-1	0.12031353e-5	0.37243609e-3	0.16757605e-0
0.11048543e-1	0.14814052e-6	0.92608080e-4	0.83400905e-1
0.55242717e-2	0.18396474e-7	0.23099315e-4	0.41611326e-1

where λ_i are basis Legendre polynomials or spline functions on $[0, 1]$, and finding the vector of coefficients $\mathbf{a}$ by inverting the linear system $\boldsymbol{M}\mathbf{a} = \mathbf{b}$ where

$$\boldsymbol{M}_{i,j} = \int_0^1 \lambda_i(y)\lambda_j(y)dy$$

and

$$b_i = \int_{\Omega_{\text{p}}(\psi_h)} r^\alpha |\nabla\psi_h|^\beta \lambda_i(\psi_{\text{N},h})|\nabla\psi_{\text{N},h}|drdz$$

For this last surface integral, as it is done for the equilibrium equation, we do not resolve the plasma domain $\Omega_{\text{p}}(\psi_h)$ but only check whether the quadrature points are inside or not.

7 Numerical results

We present some numerical results which highlight the features of the proposed method. We start by checking the correct implementation of rHCT FEs, then show an example of the use of the non-overlapping MEM for the JT60-SA tokamak. The section ends with the computation of several geometric coefficients and 1D output profiles. These last experiments are conducted with the code NICE, a C++ implementation of the methods for axisymmetric free boundary plasma equilibria described in [12].

7.1 Validation of rHCT FE implementation

Since our aim is to combine $\mathbb{P}_1$ Lagrange FEs with rHCT FEs, we can in general only expect that the global error reduction at each mesh refinement step is comparable to the error reduction of a solution without MEM, relying on $\mathbb{P}_1$ Lagrange FEs everywhere. To keep the high-order precision everywhere, we would have had to combine rHCT FEs on the exterior with high order rHCT FEs on the interior, with a large increase in the size of the system to solve. On the other hand, the use of rHCT FEs in Ω^{in} really improves the quality of the computation of interesting physical paramaters, as we will see in the following. To validate the precision of the rHCT in Ω^{in}, we consider the linear problem

$$-\nabla \cdot (\nabla u) = f \quad \text{in } \Omega^{\text{in}} = [0, 1]^2 \qquad u = u_D \quad \text{on } \mathcal{I} = \partial\Omega^{\text{in}}. \tag{30}$$

The mesh τ^{in} is a triangular one, satisfying the regularity requirements stated in [8] for the error estimate $||u - u_h||_m = O(h^{3-m})$, $m = 0, 1, 2$, with u_h the rHCT FE approximated solution of problem (30). The data f and u_D are consistent with $u(r, z) = x^4 (y - 1)^2 + y^4 (x - 1)^2$ being the solution of (30). Convergence rates (see Figure 6 and the detailed values in Table 1) are in agreement with the theoretical ones.

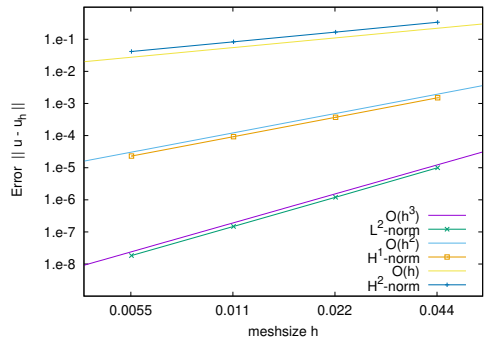

Figure 6: Error decay in $H^m(\Omega^{\text{in}})$-norm, $m = 0, 1, 2$, for the linear problem (30) using rHCT FEs on refined meshes.

7.2 JT60-SA tokamak test case

Numerical solution Numerical results for problem (8) are obtained for the configuration presented in Figure 2. The tokamak JT60SA, where JT60 stands for Japan Torus-60 and SA indicates the upgraded model with Superconducting coils, is the largest machine before ITER and is intended to be able to run with the same D-shaped plasma as ITER. The construction of the JT60SA officially began in 2013 and its assembly was completed between spring and summer 2020. The first plasma in this machine is planned for the end of 2020, it thus constitutes a perfect benchmark configuration for which numerical simulations can compute and analyse a plasma equilibrium before this equilibrium is physically generated in the machine.

Starting from the JT60-SA tokamak machine description (coils, limiter, vaccum vessel and passive structure) and a coupling interface contour , a mesh is generated using the mesh generator Triangle [32]. It is made of 6123 triangles and 3198 vertices for the external domain and 7275 triangles and 3721 vertices for the internal domain. The coupling interface contour is made of 165 vertices. Computations are initialized with an inverse static computation in the full ABB domain using $\mathbb{P}_1$ FE as implemented in the code NICE [12]. It consists in finding the currents in PF coils which enable to have a desired plasma shape. Functions p' and ff' are given through parameterization (7) where $\alpha = 2$, $\gamma = 0.8$ and $\beta = 0.5$. The scaling parameter λ is computed such that the plasma current is $I_p = 5.5 \times 10^6$ A. This provides an initial $\mathbb{P}_1$ FE equilibrium from which the coupled rHCT-$\mathbb{P}_1$ solution is initialized.

It is essential to verify numerically the implementation of the computation of the Jacobian matrix given by (23). This is done by comparison with finite differences and we check that

$$e(\varepsilon) := ||\frac{\mathbf{J}(\boldsymbol{\psi} + \varepsilon \mathbf{h}) - \mathbf{J}(\boldsymbol{\psi})}{\varepsilon} - \mathbf{Jac}_{\boldsymbol{\psi}}(\boldsymbol{\psi})\mathbf{h}|| = O(\varepsilon) \tag{31}$$

where the perturbation vector $\mathbf{h}$ is chosen randomly. Table 2 gives a typical example of such a numerical test which enables to make sure that the computation of the Jacobian is correct. The error e starts by decreasing as ε decreases. As it is typical for very small ε values, the error increases due to the accumulation of round-off errors.

This is confirmed by the good convergence of the Newton iterations (25) (see Table 3) for the resolution of the non-linear coupled problem.

The non-overlapping MEM for the $\mathbb{P}_1$-rHCT FEs' coupling works fine to reconstruct the plasma equilibrium in the tokamak (see Figure 7).

ε	e
10^0	$1.13214 \times 10^{+1}$
10^{-1}	4.94353×10^{-2}
10^{-2}	1.32271×10^{-2}
10^{-3}	3.15033×10^{-3}
10^{-4}	6.87336×10^{-5}
10^{-5}	6.61486×10^{-7}
10^{-6}	7.23428×10^{-6}
10^{-7}	7.80983×10^{-5}
10^{-8}	1.21922×10^{-3}
10^{-9}	5.06769×10^{-3}

Table 2: Convergence of the error e (Eqn (31)) for the computation of the Jacobian $\mathbf{Jac}_{\boldsymbol{\psi}}(\boldsymbol{\psi})$

n	residual relative error
1	3.47561×10^{-2}
2	2.91101×10^{-4}
3	3.32183×10^{-7}
4	1.96881×10^{-13}

Table 3: Convergence history of Newton iterations, iteration number n and residual relative error $||\mathbf{X}^n - \mathbf{X}^{n-1}||/||\mathbf{X}^{n-1}||$.

With the non-overlapping MEM we are able to introduce FE functions in Ω^{in} that are continuous with continuous derivatives, hence the location of critical points is no more restricted to a finite number of points. Indeed, we have that the plasma axis position (r_a, z_a) and the X-point position (r_b, z_b) are at points other than mesh nodes of τ^{in}, as shown with a zoom of the solution ψ_h in Figure 8, left and right, respectively.

To highlight the influence of the continuous derivatives we compare the results with the MEM that uses piece-wise linear FEs ($\mathbb{P}_1$) instead of the rHCT FEs. In Figure 9 the behavior of the poloidal component $\frac{1}{r}\nabla\psi \times \mathbf{e}_\varphi$ of the magnetic induction is shown as a function of r along the chord $\{(r, z_a),\ r_{\min} \leq r \leq r_{\max}\}$, with $r_{\min}$ (resp., $r_{\max}$) the minimum radius (resp., the maximum radius) of the tokamak vacuum chamber. The staircase effect associated with the discontinuity of the derivatives for piece-wise linear FEs is replaced by a smooth profile when rHCT FEs are adopted in Ω^{in}.

Geometric coefficients and 1D output profiles After an equilibrium is computed one can proceed with the evaluation of several output quantities which are used either to characterize the plasma (e.g the safety factor which plays a role in stating the stability of the plasma) or geometric coefficients which are use in transport models which are used to compute the quasi-static evolution of the plasma. Here we concentrate on a few 1D profiles for the computation of which we show the benefit of using rHCT FE instead of $\mathbb{P}_1$ FE.

For $\psi_{\text{N}} \in [0, 1]$, $f(\psi) = S_f(\psi_{\text{N}})$ is computed by integration of $\mathcal{B}$.

$$S_f(\psi_{\text{N}}) = [(B_0 r_0)^2 - 2(\psi_b - \psi_a)\lambda\mu_0 r_0 \int_{\psi_{\text{N}}}^1 \mathcal{B}(x)dx]^{1/2} \tag{32}$$

where B_0 is the vacuum toroidal field at $r = r_0$. For simplicity in what follows we will note $f(\psi_{\text{N}})$ for $S_f(\psi_{\text{N}})$.

Let us define a discretization of the unit interval $[0,1]$ by $S+1$ values $\psi_{\mathrm{N}}^0 = 0, \ldots, \psi_{\mathrm{N}}^S = 1$. These points are taken as abscissa for all computed 1D profiles. We also note $\Omega_{\psi_{\mathrm{N}}^s} = \{\mathbf{x} \in \Omega_{\mathrm{p}},\ \psi_{\mathrm{N}}(\mathbf{x}) \leq \psi_{\mathrm{N}}^s\}$ the domain bounded by $C_{\psi_{\mathrm{N}}^s}$.

The toroidal flux coordinate is defined and computed as

$$\rho(\psi_{\mathrm{N}}^s) = \sqrt{\phi(\psi_{\mathrm{N}}^s)/\pi B_0}$$

where

$$\phi(\psi_{\mathrm{N}}^s) = \int_{\Omega_{\psi_{\mathrm{N}}^s}} \frac{f(\psi_h(r,z))}{r} dr dz$$

Again in this last surface integral and as is done for the equilibrium equation we do not resolve the domain $\Omega_{\psi_{\mathrm{N}}^s}$ but only check if the quadrature points are inside or not.

Now that the $f(\psi_{\mathrm{N}}^s)$, $\phi(\psi_{\mathrm{N}}^s)$ and $\rho(\psi_{\mathrm{N}}^s)$ profiles are known we can proceed with other quantities. The safety factor is computed as

$$q(\psi_{\mathrm{N}}^s) = A_{-1,-1}(\psi_{\mathrm{N}}^s) \frac{f(\psi_{\mathrm{N}}^s)}{2\pi}$$

and the ψ derivative of the plasma volume as

$$\frac{\partial V}{\partial \psi}(\psi_{\mathrm{N}}^s) = -2\pi A_{1,-1}(\psi_{\mathrm{N}}^s).$$

We compute the profile $\frac{\partial \psi}{\partial \rho}(\psi_{\mathrm{N}}^s)$ as $1/\frac{\partial \rho}{\partial \psi}(\psi_{\mathrm{N}}^s)$ with $\frac{\partial \rho}{\partial \psi}(\psi_{\mathrm{N}}^s) = \frac{1}{2\pi B_0 \rho} \frac{\partial \phi}{\partial \psi}(\psi_{\mathrm{N}}^s)$ and $\frac{\partial \phi}{\partial \psi}(\psi_{\mathrm{N}}^s) = -2\pi q(\psi_{\mathrm{N}}^s)$. Once this is known we easily obtain the ρ derivative of the plasma volume

$$\frac{\partial V}{\partial \rho}(\psi_{\mathrm{N}}^s) = \frac{\partial V}{\partial \psi}(\psi_{\mathrm{N}}^s) \frac{\partial \psi}{\partial \rho}(\psi_{\mathrm{N}}^s).$$

Two important geometric coefficients are $gm_1 :=< \frac{1}{r^2} >$ and $gm_2 :=< \frac{|\nabla \rho|^2}{r^2} >$ computed as

$$gm_1(\psi_{\mathrm{N}}^s) = \frac{A_{-1,-1}(\psi_{\mathrm{N}}^s)}{A_{1,-1}(\psi_{\mathrm{N}}^s)}, \qquad gm_2(\psi_{\mathrm{N}}^s) = (\frac{\partial \rho}{\partial \psi}(\psi_{\mathrm{N}}^s))^2 \frac{A_{-1,1}(\psi_{\mathrm{N}}^s)}{A_{1,-1}(\psi_{\mathrm{N}}^s)}.$$

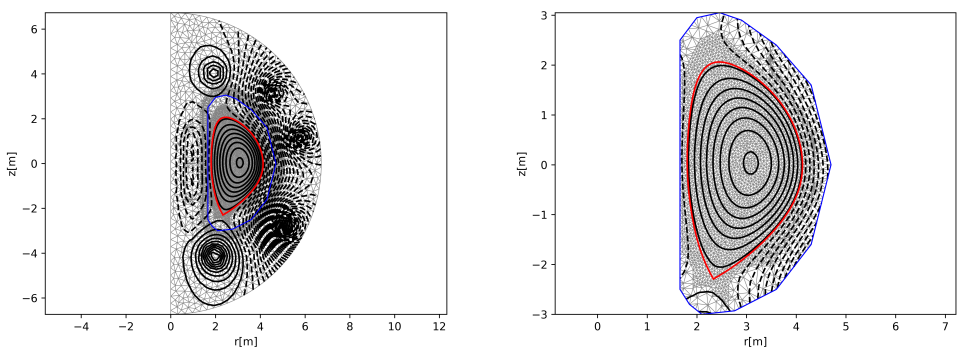

Figure 7: Iso-contours of ψ_h in the whole domain Ω (left) and in Ω_{L} (right), computed by the proposed non-overlapping MEM to have $\mathbb{P}_1$ FEs in Ω^{ex} and rHCT FEs in Ω^{in}.

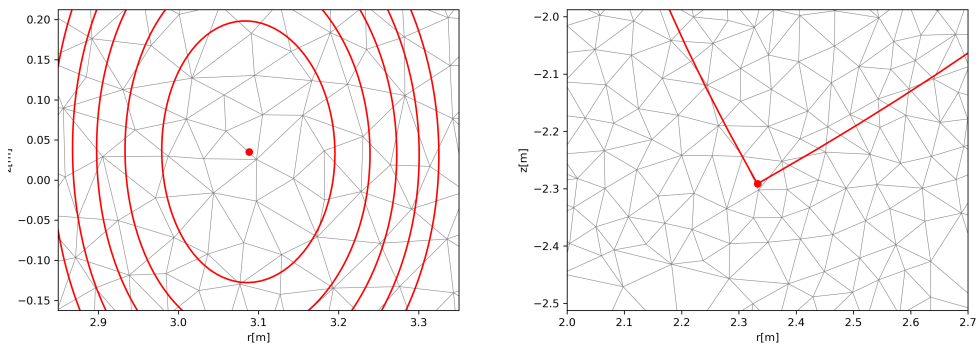

Figure 8: A zoom of the iso-contours of ψ_h in Ω_{L}, with the plasma axis (left) and X-point (right) localization.

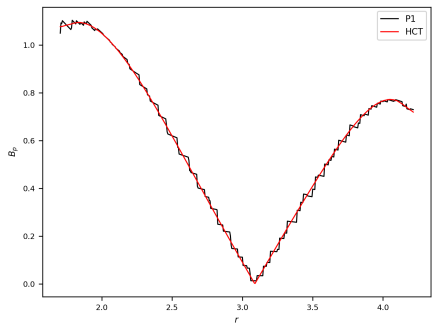

Figure 9: Poloidal magnetic field $||\nabla\psi(r, z_a)||/r$ as a function of r in the vacuum vessel. In black the $\mathbb{P}_1$ solution and in red the rHCT solution

Among the many other quantities that can be computed out from an equilibrium configuration we are only going to examine one more, the magnetic shear profile defined as $sh := \dfrac{\rho}{q}\dfrac{\partial q}{\partial \rho}$ which is difficult to compute smoothly because of the q derivative. This derivative is approximated using centered finite differences.

Figure 10 shows these computed profiles for 4 different cases: the $\mathbb{P}_1$ FE case and three rHCT cases, using the isocontour method or the weak formulation method with either Legendre polynomials or splines in order to compute integrals $A_{\alpha,\beta}$. As expected profiles computed from the rHCT solution are smoother than those computed from the $\mathbb{P}_1$ solution. This is particularly clear for example for gm_2 close to the magnetic axis ($\psi_{\mathrm{N}} = 0$) or for the magnetic shear. Profiles computed from the rHCT solution with three different numerical methods differ very little. Concerning the computation time it can be noted that these runs were done on a laptop with two dual cores using `OpenMP` to parallelize the isocontour computations. Despite this, the weak formulation method is still faster than the isocontour method.

8 Conclusion

In this paper we propose a numerical method which enables the computation of a high order approximation of the equilibrium of the plasma in a tokamak. The method relies on the decomposition of the computational domain in two subdomains, the external one, not containing the plasma and in which $\mathcal{C}^0$ piece-wise linear Lagrange FEs are used, and the internal one, containing the plasma in which $\mathcal{C}^1$ rHCT FEs are used. The coupling between the two subdomains is done thanks to a mortar element method for which we showed that the L^2-projection method enables to ensure an excellent transmission of information from one domain to the other. At the discrete level we propose a Newton method to solve the coupled nonlinear problem and give numerical evidence of its convergence. We also propose two different approaches to compute the geometric coefficients which are essential outputs of a plasma equilibrium computation. The second one, based on a variational formulation over the plasma domain is fast and precise. It does not require the explicit computation of iso-contours as the first method does.

Acknowledgements

This work is supported by the French National Research Agency grant SISTEM (ANR-19-CE46-0005-03). The first and second authors have worked within the framework of the EURO Fusion Consortium and have received funding from Euratom research and training programs 2014-2018, 2019-2020, under the grant agreement N.633053. The views and opinions expressed herein do not necessarily reflect those of the European Commission. The third author thanks the project team CASTOR at INRIA for the delegation in 2020, during which this work was completed.

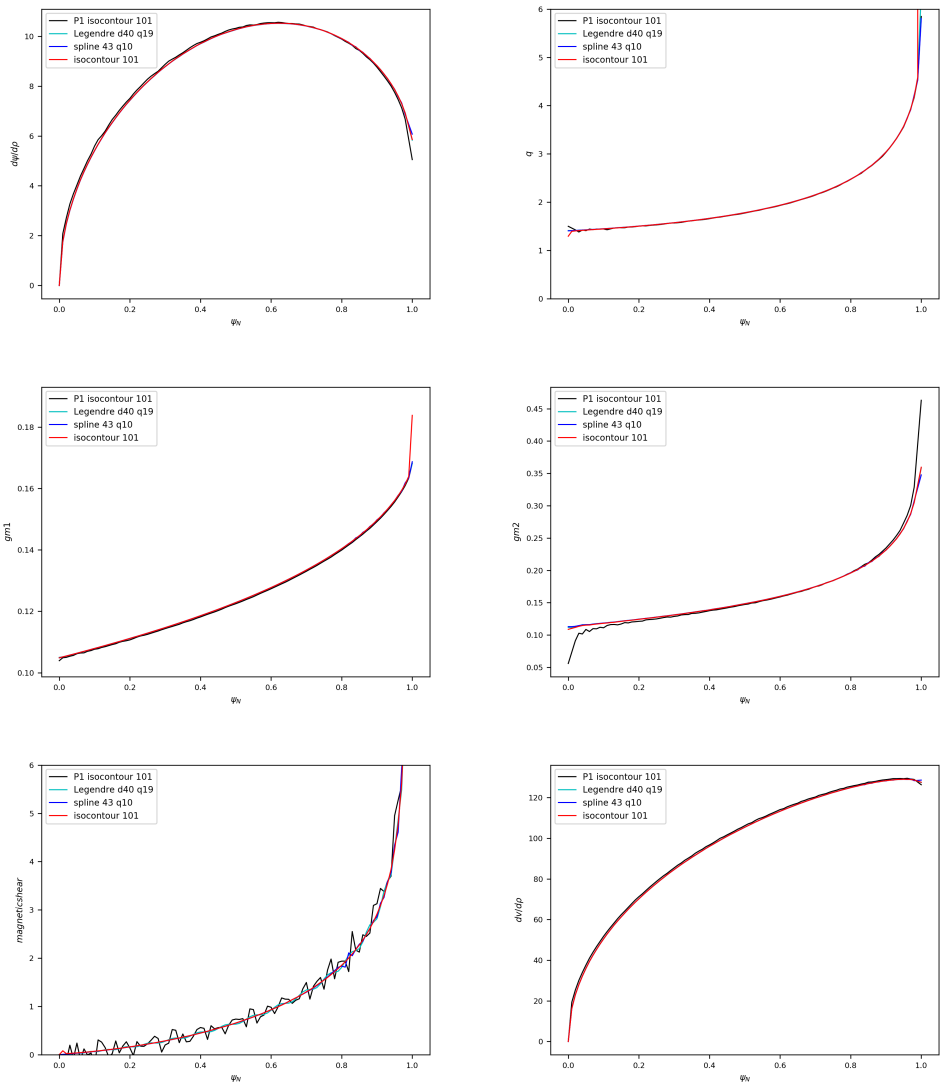

Figure 10: The profile of $\dfrac{\partial \psi}{\partial \rho}(\psi_{\mathrm{N}})$ (top, left), $q(\psi_{\mathrm{N}})$ (top, right), $gm_1(\psi_{\mathrm{N}})$ (center, left), $gm_2(\psi_{\mathrm{N}})$ (center, right), $sh(\psi_{\mathrm{N}})$ (bottom, left) and of $\dfrac{\partial V}{\partial \rho}(\psi_{\mathrm{N}})$ (bottom, right). Black: 101 iso-contours method from the $\mathbb{P}_1$ solution. Red: 101 iso-contours method from the rHCT solution. Cyan: weak formulation method with Legendre polynomials up to degree 40 and a quadrature rule of order 19. Blue: weak formulation method with 43 splines and a quadrature of order 10.

References

[1] R. Albanese, J. Blum, and O. Barbieri. On the solution of the magnetic flux equation in an infinite domain. In *EPS. 8th Europhysics Conference on Computing in Plasma Physics (1986)*, pages 41–44, 1986.

[2] Henri Berestycki and Haïm Brézis. On a free boundary problem arising in plasma physics. *Nonlinear Anal.*, 4(3):415–436, 1980.

[3] C. Bernardi, Y. Maday, and A.T. Patera. A new nonconforming approach to domain decomposition: The mortar element method. In *Nonlinear Partial Differential Equations and Their Applications.* in H. Brézis and J.-L. Lions (eds.), Collège de France Seminar XI., 1992.

[4] C. Bernardi, Y. Maday, and F. Rapetti. Basics and some applications of the mortar element method. *GAMM-Mitt.*, 28:97–123, 2005.

[5] M. Bernardou and K Hassan. Basis functions for general Hsieh-Clough-Tocher triangles, complete or reduced. Research Report RR-0005, INRIA, 1980. `https://hal.inria.fr/inria-00076556`.

[6] J. Blum. *Numerical Simulation and Optimal Control in Plasma Physics with Applications to Tokamaks.* Series in Modern Applied Mathematics. Wiley Gauthier-Villars, Paris, 1989.

[7] J. Blum, T. Gallouet, and J. Simon. Existence and control of plasma equilibrium in a tokamak. *SIAM Journal on Mathematical Analysis*, 17(5):1158–1177, 1986.

[8] P. G. Ciarlet. *The Finite Element Method for Elliptic Problems.* North-Holland Publishing Co., Amsterdam, 1978. Studies in Mathematics and its Applications, Vol. 4.

[9] R.W. Clough and J.L. Tocher. Finite element stiffness matrices for analysis of plates in bending. In *Proc. Conf. Matrix Methods in Struct. Mech.*, Air Force Inst of Tech., Wright Patterson A.F Base, Ohio, October 1965.

[10] Lukas Drescher, Holger Heumann, and Kersten Schmidt. A high order method for the approximation of integrals over implicitly defined hypersurfaces. *SIAM Journal on Numerical Analysis*, 55(6):2592–2615, 2017.

[11] G.L. Falchetto, D. Coster, R. Coelho, B.D. Scott, L. Figini, D. Kalupin, E. Nardon, S. Nowak, L.L. Alves, J.F. Artaud, V. Basiuk, Jo ao P.S. Bizarro, C. Boulbe, A. Dinklage, D. Farina, B. Faugeras, J. Ferreira, A. Figueiredo, Ph. Huynh, F. Imbeaux, I. Ivanova-Stanik, T. Jonsson, H.-J. Klingshirn, C. Konz, A. Kus, N.B. Marushchenko, G. Pereverzev, M. Owsiak, E. Poli, Y. Peysson, R. Reimer, J. Signoret, O. Sauter, R. Stankiewicz, P. Strand, I. Voitsekhovitch, E. Westerhof, T. Zok, W. Zwingmann, ITM-TF Contributors, the ASDEX Upgrade Team, and JET-EFDA Contributors. The European Integrated Tokamak Modelling (ITM) effort: achievements and first physics results. *Nuclear Fusion*, 54(4):043018, 2014.

[12] B. Faugeras. An overview of the numerical methods for tokamak plasma equilibrium computation implemented in the NICE code. *Fusion Eng. Design*, 160:112020, 2020.

[13] B. Faugeras and H Heumann. FEM-BEM coupling methods for tokamak plasma axisymmetric free-boundary equilibrium computations in unbounded domains. *J. Computational Physics*, 343(Supplement C):201 – 216, 2017.

[14] Herbert Federer. *Geometric measure theory.* Die Grundlehren der mathematischen Wissenschaften, Band 153. Springer-Verlag New York Inc., New York, 1969.

[15] J. P. Freidberg. *Ideal Magnetohydrodynamics.* Plenum US, 1987.

[16] Johan P Goedbloed, Rony Keppens, and Stefaan Poedts. *Advanced magnetohydrodynamics: with applications to laboratory and astrophysical plasmas.* Cambridge University Press, 2010.

[17] Johan Peter Goedbloed and Stefaan Poedts. *Principles of magnetohydrodynamics: with applications to laboratory and astrophysical plasmas.* Cambridge university press, 2004.

[18] H. Grad and J. Hogan. Classical diffusion in a tokomak. *Phys. Rev. Lett.*, 24:1337–1340, Jun 1970.

[19] H. Grad and H. Rubin. Hydromagnetic equilibria and force-free fields. *Proceedings of the 2nd UN Conf. on the Peaceful Uses of Atomic Energy*, 31:190, 1958.

[20] Virginie Grandgirard. *Modélisation de l'équilibre d'un plasma de tokamak.* PhD thesis, Université de Franche-Comté, 1999.

[21] Z. Jiang H. Haddar and A. Lechleiter. Artificial boundary conditions for axisymmetric eddy current probe problems. *Computers & Mathematics with Applications*, 68(12A):1844–1870, 2014.

[22] H. Heumann, J. Blum, C. Boulbe, B. Faugeras, G. Selig, J.-M. Ané, S. Brémond, V. Grandgirard, P. Hertout, and E. Nardon. Quasi-static free-boundary equilibrium of toroidal plasma with CEDRES++: Computational methods and applications. *Journal of Plasma Physics*, 81, 6 2015.

[23] H. Heumann and F. Rapetti. A finite element method with overlapping meshes for free-boundary axisymmetric plasma equilibria in realistic geometries. *J. Computational Physics*, 334:522–540, 2017.

[24] F.L. Hinton and R.D. Hazeltine. Theory of plasma transport in toroidal confinement systems. *Rev. Mod. Phys.*, 48:239–308, Apr 1976.

[25] S.C. Jardin. A triangular finite element with first-derivative continuity applied to fusion mhd applications. *J. Comput. Phys.*, 200(1):133–152, October 2004.

[26] S.C. Jardin. *Computational methods in plasma physics.* Boca Raton, FL : CRC Press/Taylor & Francis, 2010.

[27] R. Lüst and A. Schlüter. Axialsymmetrische magnetohydrodynamische Gleichgewichtskonfigurationen. *Z. Naturforsch. A*, 12:850–854, 1957.

[28] J.N. Lyness and D. Jespersen. Moderate degree symmetric quadrature rules for the triangle. *J. Inst. Maths. Applics.*, 15:19–32, 1975.

[29] Leszek Marcinkowski. *Mortar methods for some second and fourth order elliptic equations.* PhD thesis, 1999.

[30] Masa Aki Nakamura. On an equilibrium of the plasma in a tokamak with a limiter. *Japan Journal of Industrial and Applied Mathematics*, 8(3):431–444.

[31] V.D. Shafranov. On magnetohydrodynamical equilibrium configurations. *Soviet Journal of Experimental and Theoretical Physics*, 6:545, 1958.

[32] J.R. Shewchuk. Triangle: Engineering a 2D Quality Mesh Generator and Delaunay Triangulator. In Ming C. Lin and Dinesh Manocha, editors, *Applied Computational Geometry: Towards Geometric Engineering*, volume 1148 of *Lecture Notes in Computer Science*, pages 203–222. Springer-Verlag, May 1996. From the First ACM Workshop on Applied Computational Geometry.

[33] R. Temam. Remarks on a free boundary value problem arising in plasma physics. *Comm. Partial Differential Equations*, 2(6):563–585, 1977.

[34] J. Wesson. *Tokamaks*. The International Series of Monographs in Physics. Oxford University Press, 2004.

RESEARCH CENTRE
SOPHIA ANTIPOLIS – MÉDITERRANÉE

2004 route des Lucioles - BP 93
06902 Sophia Antipolis Cedex

Publisher
Inria
Domaine de Voluceau - Rocquencourt
BP 105 - 78153 Le Chesnay Cedex
inria.fr

ISSN 0249-6399